On the Origin of Hypervelocity Stars

Karl W Jansson

Lund Observatory
Lund University

2010-EXA43

Degree project of 15 higher education credits
June 2010

Lund Observatory
Box 43
SE-221 00 Lund
Sweden

On the Origin of Hypervelocity Stars

Karl W Jansson
Lund Observatory
Lund University

June 30, 2010

Abstract

Hypervelocity stars (HVSs) are stars located in the Galactic halo travelling with extremely high speeds. They are produced when a binary approches the supermassive black hole (SMBH) in the Galactic Center (GC) and gets tidally broken up. In this process one of the stars is ejected with high velocity.

The angle between the velocity of the incoming binary and the velocity of the ejected HVS is almost 180°. Lu et al. (2010) claims that all the HVSs come from two distinctive existing disks of stars by stating that the planar structure of the stars is preserved since the deflection angle is 180°.

I derive different properties of HVSs, e.g. the deflection angle and the break-up radii as functions of the SMBH mass, the initial velocity of the binary, the ejection velocity, the closest approach of the binary, the binary separation, the stellar radii and the stellar masses. I also discuss what happens to the other star in the binary and the future of the HVSs.

I test the results of Lu et al. (2010) by trying to find combinations of two planes that have a better fit than their results. I also use a larger sample of stars than they do and also I consider the effects of the Galactic potential on the trajectories of the HVSs.

My conclusions are that there exist many more combinations of two planes that fit the origin of the HVSs better than the two existing disks so it is not really possible to claim that the HVSs come from these two disks.

In the final section I discuss what happens if you change some parameters, the SMBH mass and the binary separation, and also how you could extend the project in the future, e.g. if you add post-Newtonian effects and if there is an assymmetric dark matter halo in the Milky Way.

Contents

1 Introduction to the HVSs

In the restframe of our Galaxy the Sun has a velocity of $v_{\odot,rf} \approx 220$ km s^{-1}. Other stars have velocities of the same order or smaller as seen from Figure 1.

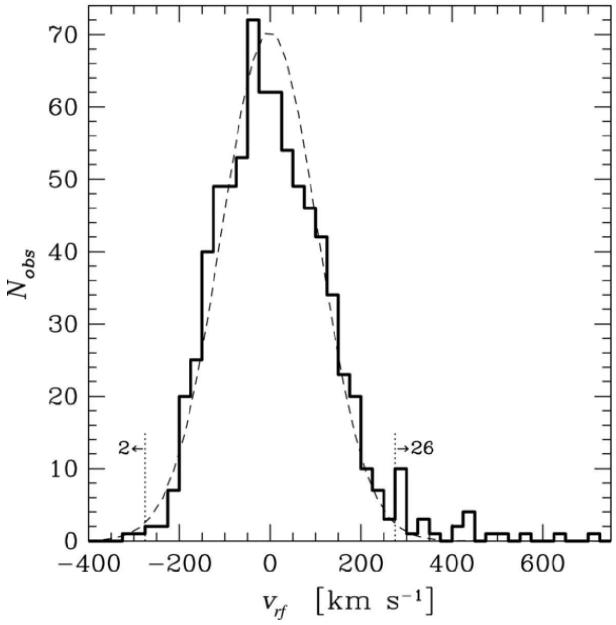

Figure 1: Minimum Galactic rest-frame velocity v_{rf} distribution of the HVS survey by Brown et al. (2009), the figure is taken from their paper. Notable is that there are 26 stars with $v_{rf} > 275$ km s^{-1} and only 2 stars with a rest-frame velocity < -275 km s^{-1}.

Our Galaxy consists of three parts: a disk, a bulge and a halo. In the Milky Way star formation occurs mostly in the disk and bulge while the halo mostly consists of older stars. Since stellar evolution is dependant on the mass of the star, more massive stars evolve more quickly so old stars have a low mass. Low mass stars also are cooler and have a a reddish colour while massive stars are blue since they are hotter. Yet blue objects have been discovered in the halo at galactocentric distances of ∼15-125 kpc (Brown et al., 2005). Blue stars are either massive main sequence stars (MS-stars) or less massive blue horizontal branch stars (BHB-stars). The dopplershift of the stars shows that all stars move away from the Galaxy with high velocities, $v_{rf} > 275$ km s^{-1}, comparable to or larger than the escape velocity of the Galaxy. Svensson et al. (2008) showed that some of the stars are bound to the Galaxy with an orbital period of about 2 Gyr. Since all stars move away from the GC they deduce that the lifetimes of the stars are smaller than 2 Gyr and hence deduce that the stars are massive MS-stars rather than BHB-stars. Because if they were BHB-stars some stars would probably have been seen returning to the GC since a less massive star can have MS-lifetimes larger than 2 Gyr and they could evolve into BHB-stars when they return to the GC and hence be seen with a negative radial velocity. If you assume the stars to be 3 $M_\odot$ MS-stars and use the apparent magnitude of the star you can get the distance to the star.

The stars are found in the Sloan Digital Sky Survey (SDSS)-catalogue by selecting late B-type stars. What is a B-type star then? One way to classify stars is to order them depending on the temperature of the star. Usually you sort them into seven groups labelled by the letters O, B, A, F, G, K and M where O-stars are the hottest and stars of the following letters gradually get cooler down to the coolest M-stars, so B-stars are hot, blue stars. The

survey covers $\sim$ 7300 deg^2 or 17.7 % of the sky. But not areas close to the Galactic bulge since that area is contaminated by stars not belonging to the halo (Brown et al., 2009). Brown et al. (2009) took the spectra of the stars in the survey to get the radial velocities and selected the ones with $v_{rf} > 275$ km s^{-1}. As you can see in Figure 1 it's not a large fracion of the whole sample.

These blue high-speed objects are called hypervelocity stars, their properties are given in Table 1. So far 32 HVSs have been found. I have divided them into four different categories. Three categories are the ones in Brown et al. (2009) where they are separated depending on their Galactic restframe velocity compared to the escape velocity at their location. The final category is the stars included in Svensson et al. (2008) but not in Brown et al. (2009).

Table 1: Table of all HVSs I have used in my simulations. If the ID of the star does not start with the letter J it's not from the SDSS-catalogue but from some other. M_V is the absolute magnitude of the star, R_{GC} is the galactocentric distance, b_{GC} is the longitude of the star in a SMBH centered coordinate system, l_{GC} is the longitude in the same system, v_{rf} is the velocity in the rest frame of the Galaxy. The final two columns are the change in longitude, $\Delta l = l_{GC} - l_{ej}$, and latitude, $\Delta b = b_{GC} - b_{ej}$, of the HVSs due to the Galactic potential. The data for the first three groups of HVSs is taken from Brown et al. (2009) and the data for the Svensson HVSs is taken from Brown et al. (2007). The data for HE 0437-5439 is taken from Edelmann et al. (2005). The coordinates have been transformed from Galactic coordinates to a reference system centered in the Galactic Center.

Star ID (SDSS)	R_{GC} (kpc)	b_{GC} (deg)	l_{GC} (deg)	v_{rf} (km/s)	Δl (deg)	Δb (deg)
HVSs						
J090744.99+024506.9	111	29.81	223.78	696	0.01	-2.24
US 708	26	33.89	177.49	717	0.00	-2.94
HE 0437-5439	62	-39.90	253.31	548	0.00	1.48
J091301.01+305119.8	82	38.84	192.91	566	0.05	-3.58
J091759.48+672238.3	45	33.12	153.09	649	-0.01	-2.97
J110557.45+093439.5	78	56.85	233.37	528	-0.05	-2.03
J113312.12+010824.9	60	56.44	249.78	416	-0.03	-2.34
J094214.04+200322.1	53	40.76	205.61	407	-0.02	-4.63
J102137.08-005234.8	68	42.02	236.30	485	0.01	-2.70
J120337.85+180250.4	87	73.19	232.33	432	-0.21	-1.47
J095906.48+000853.4	70	38.16	231.53	336	0.05	-4.49
J105009.60+031550.7	70	50.01	237.56	429	0.03	-2.86
J105248.31-000133.9	125	49.61	246.20	443	0.10	-2.45
J104401.75+061139.0	112	51.84	235.91	416	-0.13	-2.92
J113341.09-012114.2	85	54.88	252.08	343	0.00	-2.89
J122523.40+052233.8	90	68.14	267.59	367	0.09	-1.84
Possible HVSs						
J094014.56+530901.7	65	41.36	165.77	279	-0.02	-6.06
J101359.79+563111.7	79	45.33	158.96	289	-0.10	-5.34
J140306.54+145005.0	59	76.66	0.22	289	0.06	-1.29
J154556.10+243708.9	83	54.08	45.42	293	-0.03	-1.32
Possible Bound HVSs						
J032054.69-530901.7	40	-40.08	186.75	279	0.02	6.39
J074950.24+243841.2	66	20.53	193.99	298	-0.02	-8.63
J081828.07+570922.1	42	28.26	164.65	288	-0.02	-8.14
J090710.08+365957.5	57	36.71	185.19	285	-0.04	-6.95
J110224.37+025002.8	51	51.12	237.34	331	-0.02	-3.71
J115245.91-021116.2	53	57.03	258.63	310	0.01	-3.01
J140432.38+352258.4	39	73.26	106.27	298	-0.09	-2.40
J141723.34+101245.7	49	72.12	357.98	290	-0.08	-1.75
Svensson HVSs						
J075055.24+472822.9	42	24.01	173.29	312	0.00	-8.46
J075712.93+512938.0	32	23.57	170.56	341	0.00	-8.20
J142001.94+124404.8	27	80.51	7.05	372	-0.04	-0.83
J144955.58+310351.4	16	66.58	58.18	644	0.02	-1.48

The idea is that they come from the GC and are produced in three-body interactions between a binary and the SMBH.

2 How they are made

2.1 Production mechanism

The production mechanism of HVSs were first suggested by Hills (1988) several years before the first HVS was discovered in 2005 (Brown et al., 2005). The idea is that a binary approaches the SMBH. That leads to a tidal break-up of the binary in which one of the stars is captured in a very tightly bound, highly eccentric orbit around the SMBH. In this process the star loses a lot of energy, but the total energy should be conserved so the other star gets the extra energy and is ejected with a very high velocity, hence the name HVS.

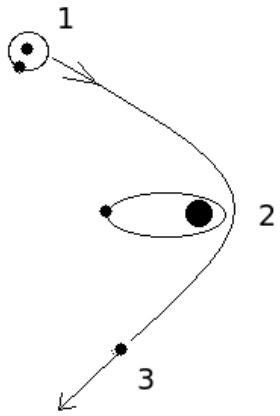

Figure 2: Production mechanism of HVSs. A binary approaches the SMBH (1). The binary is tidally broken up and one of the stars becomes tightly bound to the SMBH (2). The other star is ejected with high velocity, this is the HVS (3).

As discussed earlier in Section 1 some of the HVSs are bound to the Galaxy and since all HVSs move away from the GC I assume them to be quite massive MS-stars. I can make an approximation of the ejection speed, v_{ej}, of the HVSs. For simplicity I assume an equal mass binary, i.e. the two stars in the binary has the same mass.

$$E_{before} \approx -G\frac{M_\star^2}{2a_{bin}}$$

$$E_{after} = -G\frac{M_\star M_{BH}}{2a_{BH}} + \frac{M_\star v_{ej}^2}{2}$$

$$E_{before} = E_{after} \Longrightarrow \frac{M_\star v_{ej}^2}{2} = \frac{GM_\star}{2}\left(\frac{M_{BH}}{a_{BH}} - \frac{M_\star}{a_{bin}}\right)$$

$$\Longrightarrow v_{ej} = \sqrt{G\left(\frac{M_{BH}}{a_{BH}} - \frac{M_\star}{a_{bin}}\right)} \approx \sqrt{G\frac{M_{BH}}{a_{BH}}} \sim 800 \text{ km s}^{-1} \quad (1)$$

We neglect the second term under the root since the mass of the SMBH is so much larger than that of a HVS, $\sim 3.5 \times 10^6$ $M_\odot$ compared to ~ 3 $M_\odot$. I use $a_{BH} \approx 5000$ au (Svensson et al., 2008).

Normal star speed is of the order 100 km s^{-1} (see Figure 1), e.g. $v_\odot \sim 220$ km s^{-1} compared to the HVSs which have velocities of the order 1000 km s^{-1}. Is there anything else that is special with these stars? Yes, the ejection velocity of the HVS and the direction of the incomming binary is almost anti-parallel, i.e the deflection angle is $\sim 180°$.

2.2 The deflection angle of a HVS

So I claim that the deflection angle is 180°, how do I show that? I set the incoming binary on a hyperbolic orbit with $R_{min} \ll a$, where R_{min} is the closest distance to the SMBH and a is the semi-major axis of the orbit of the binary around the SMBH.

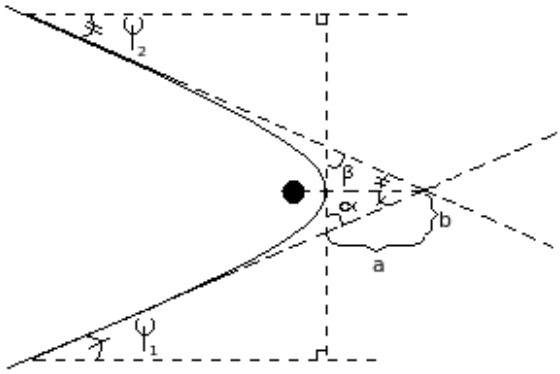

Figure 3: The total deflection, θ, is $\alpha + \beta$. a is the semi-major axis and b is the semi-minor axis of the orbit.

I split deflection in two parts, the total deflection is $\theta = \alpha + \beta$:

$$\alpha = \frac{\pi}{2} - \psi_1$$

$$\tan\psi_1 = \frac{b}{a}$$

the eccentricity of a hyperbola is, by definition,

$$e = \sqrt{1 + \frac{b^2}{a^2}} \Longrightarrow \tan\psi_1 = \sqrt{e^2 - 1}$$

the closest distance, R_{min}, between the binary and the SMBH is

$$R_{min} = e \cdot a - a \Longrightarrow e = \frac{R_{min}}{a} + 1$$

$$\Longrightarrow \tan\psi_1 = \sqrt{\left(\frac{R_{min}}{a}\right)^2 + 2\frac{R_{min}}{a} + 1 - 1} \approx \sqrt{2\frac{R_{min}}{a}} \tag{2}$$

since $R_{min} \ll a$. Energy is constant so at "infinity":

$$\left.\begin{array}{rcl} E & = & \frac{m_\star \left(v_\infty^{in}\right)^2}{2} \\ E & = & G\frac{M_{BH} m_\star}{2a} \end{array}\right\} \Longrightarrow a = G\frac{M_{BH}}{\left(v_\infty^{in}\right)^2}$$

inserting in eq. (2) yields

$$\tan\psi_1 \approx v_\infty^{in}\sqrt{\frac{2R_{min}}{GM_{BH}}}$$

I get β in similar way but I change v_∞^{in} to v_∞^{HVS} which is the velocity oft the HVS at "infinity". Then the total deflection becomes

$$\theta = \alpha + \beta = \pi - (\psi_1 + \psi_2)$$

$\tan\psi_2$ is small even for large v_∞^{in} so $\tan\psi_2 \approx \psi_2$. Also $\tan\psi_1 \approx \psi_1$ but we neglect ψ_1 since $v_\infty^{in} \ll v_\infty^{HVS}$. With $v_\infty^{HVS} \sim 700$ km/s at the current location, $R_{min} \approx 100$ au (see Section 2.3) and $M_{BH} \approx 3.5 \times 10^6$ $M_\odot$ we get $\psi_2 \approx 0.23 \sim 13°$.

$$\theta \approx \pi - \sqrt{\frac{2R_{min}}{GM_{BH}}}\left(v_\infty^{HVS} + v_\infty^{in}\right) \approx 170° \tag{3}$$

i.e. the ejection direction is almost anti-parallel to the initial binary velocity. This holds somewhat for parabolic trajectories and elliptical orbits with $e \approx 1$, but v_∞ can't be the velocity of the star at the apoapsis.

The interesting thing with the fact that the deflection angle is almost 180° is that if we know where the stars are now we automatically know from which direction from the SMBH they come from.

2.3 Tidal disruption radius, r_{bt}, of a binary

To be able to create a HVS the binary must come close enough to the SMBH so the tidal forces can break the binary. Here I show my calculations of the tidal disruption radius, r_{bt}.

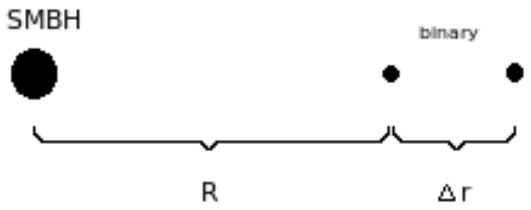

Figure 4: Tidal disruption of a binary. R is the distance from the SMBH to the star closest to it. Δr is the binary separation.

The force on the star closest to the SMBH is

$$F(R) = G\frac{M_{BH}\frac{m_b}{2}}{R^2} \tag{4}$$

the force on the other star becomes

$$F(R+\Delta r) = G\frac{M_{BH}m_b}{2(R+\Delta r)^2} = G\frac{M_{BH}m_b}{2R^2}\frac{1}{\left(1+\frac{\Delta r}{R}\right)^2} =$$

$$= G\frac{M_{BH}m_b}{2R^2} - \frac{GM_{BH}m_b}{R^3}\Delta r + \mathcal{O}\left(\left(\frac{\Delta r}{R}\right)^2\right) \tag{5}$$

where we have used $\Delta r \ll R$. The difference between eq. (4) and eq. (5) is the tidal force, F_t.

$$F_t \approx G\frac{M_{BH}m_b}{R^3}\Delta r \tag{6}$$

The force on one of the stars due to the other is

$$F_G = G\frac{m_b m_b}{4(\Delta r)^2} \tag{7}$$

When eq. (6) is equal to eq. (7) we get the tidal disruption radius, $R = r_{bt}$, of the binary

$$G\frac{M_{BH}m_b}{r_{bt}^3}\Delta r \approx G\frac{m_b^2}{4(\Delta r)^2} \Longrightarrow r_{bt} \approx \left(4\frac{M_{BH}}{m_b}\right)^{1/3}\Delta r \tag{8}$$

Using a SMBH mass of $M_{BH} \sim 3.5\times10^6$ $M_\odot$, a binary mass of $m_b \sim 6$ $M_\odot$ and a binary separation of $\Delta r \sim 1$ au I get a binary disruption radius of ~ 100 au, which is the reason I used that value when I calculated the deflection angle in eq. 3.

2.4 Tidal disruption radius, r_t, of a single star

So the binary needs to come close to the SMBH to get broken up but if it comes too close the stars in the binary can be disrupted themselves.

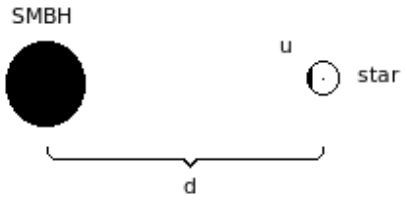

Figure 5: Tidal disruption of a single star. d is the distance from the center of the star to the SMBH. u is a small mass element in the star.

The force on mass element u at the surface of a star from the rest of the star is

$$F_G = G\frac{m_\star u}{r_\star^2} \tag{9}$$

If u is the part of the star that is closest to the SMBH, then the force on u from the SMBH is,

$$F_{BH,1} = G\frac{M_{BH}u}{(d-r_\star)^2} = G\frac{M_{BH}u}{d^2}\frac{1}{\left(1-\frac{r}{d}\right)^2} =$$

$$= G\frac{M_{BH}u}{d^2} + 2G\frac{M_{BH}u}{d^3}r + \mathcal{O}\left(\left(\frac{r}{d}\right)^2\right) \tag{10}$$

The force on a mass element u in the middle of the star from the SMBH is

$$F_{BH,2} = G\frac{M_{BH}u}{d^2} \tag{11}$$

The difference between eq. (10) and eq. (11) is the tidal force, F_t

$$F_t \approx 2G\frac{M_{BH}u}{d^3}r \tag{12}$$

When eq. (12) is equal to eq. (9) we reach the Roche limit, tidal disruption, then $d = r_t$.

$$G\frac{m_\star u}{r_\star^2} \approx 2G\frac{M_{BH}u}{r_t^3}r_\star \Longrightarrow r_t \approx \left(2\frac{M_{BH}}{m_\star}\right)^{1/3} r_\star \tag{13}$$

From Antonini et al. (2010) $r_\star \propto m_\star^{0.75}$ which leads to $r_t \propto m_\star^{3/4-1/3} = m_\star^{5/12}$, i.e. r_t is larger for more massive stars. To get an idea of the difference between r_{bt} and r_t we do an approximation of the tidal disruption radius of a 3 $M_\odot$-star. Using the mass-radius relation above we get $r_\star \sim 2.3$ $R_\odot$ which yields $r_t \sim 300$ $R_\odot \sim 1.4$ au compared to $r_{bt} \sim 100$ au.

2.5 Limits on initial velocity, v_{in}

There are some limits on the initial velocity or to be more precise the angular momentum of the incomming binary. This matters because it determines how close to the SMBH the binary will come

Small $v_{in} \Longrightarrow$ periapsis close to the SMBH.

High $v_{in} \Longrightarrow$ peirapsis far from the SMBH.

where the periapsis is the smallest distance to the SMBH in the orbit of the binary. To get the limits I let the binary start in a highly eccentric elliptical orbit with semi-major axis a, binary mass m and a distance to SMBH d. The energy in the binary is then

$$E = \frac{mv^2}{2} - G\frac{M_{BH}m}{d}$$

but also

$$E = -G\frac{M_{BH}m}{2a}$$

If I take d to be the distance at almost "infinity", apoapsis, then we get

$$\frac{mv_{in}^2}{2} = GM_{BH}m\left(\frac{1}{d} - \frac{1}{2a}\right) \Longrightarrow v_{in} = \sqrt{GM_{BH}\left(\frac{2}{d} - \frac{1}{a}\right)}$$

For an ellipse we have $2a = d + r_{per}$. Then I get

$$v_{in} = \sqrt{GM_{BH}\left(\frac{2}{d} - \frac{2}{d + r_{per}}\right)} = \sqrt{GM_{BH}\frac{d + r_{per} - d}{d\,(d + r_{per})}} =$$

$$= \sqrt{\frac{2GM_{BH}}{d^2/r_{per} + d}} \tag{14}$$

This way we get constraints on v_{in}. To get an ejection of a HVS the binary needs to pass between r_t and r_{bt}. So from eq. (14) I get

$$v_{in,min} = \sqrt{\frac{2GM_{BH}}{d^2/r_t + d}}$$

$$v_{in,max} = \sqrt{\frac{2GM_{BH}}{d^2/r_{bt} + d}}$$

If I use a SMBH mass of $M_{BH} \sim 3.5 \times 10^6$ $M_\odot$ and a apoapsis distance of $d \sim 0.01$ pc (Antonini et al., 2010) I get the limits on the initial velocity to be $v_{in,min} \sim 45$ km s^{-1} and $v_{in,max} \sim 370$ km s^{-1}.

2.6 The orbits of the HVSs

The Milky Way consists of three parts: a disk, a bulge and a halo, where the bulge and especially the disk are not spherically symmetric. Because of this the potential of the Milky Way isn't spherically symmetric and the HVSs will not only be slowed down but also the direction to the HVSs as seen from the SMBH will be changed by it. If the potential had been spherically symmetric the HVSs would only have been slowed down. The most asymmetric part is the disk and the orbits will be bent towards the disk. The result of this is that the apparent location/direction of a HVS today isn't the same as the direction it was once ejected.

2.7 The captured stars

What about the captured stars? One theory is that these stars are the so called S-stars. The S-stars are a group of stars orbiting Sgr A* (i.e. the SMBH) in very tight orbits, within 0".5($\sim$ 0.02 pc), their orbits are very eccentric. The S-stars are mainly B-type stars so they are in the same mass range as the HVSs. The high mass of the SMBH and the high eccentricity of the S-stars make the orbital period short and for a lot of the S-stars a large fraction of the orbit has been observed. Because of this the S-stars serve as a good tool for measuring the mass of the SMBH (Eisenhauer et al. (2005), Svensson et al. (2008)). One more reason the S-stars are considered to be the captured stars from the binary break-up is that since they are so close to the SMBH star formation there is impossible because of the SMBH's tidal fields. So they have to originate some other place in the Galaxy and then it could be so that they are the captured stars (Davies and King, 2005). Also the large orbital eccentricities are consistent with the idea that they are the captured stars.

3 The point of my project

Now I have described what a HVS is, how they are made and some other properties of them but I have yet to say what the point of the project is. For my project I start from the work of Lu et al. (2010). They claim that all HVSs originate from two separate planes or rather disks and that these two disks are consistent with two existing disks in the GC

- The clockwise-rotating young stellar disk (CWS) located ~ 0.5 pc from the SMBH (Paumard et al., 2006).
- The Northern arm (Narm), a gaseous structure within a few pc of the GC. The northern arm orbits around Sgr A* and has a high eccentricity ~ 0.8. It is a part of the mini-spiral in the GC which contians ionized gas "arms" (Zhao et al., 2009).

They use the 16 "confirmed" HVSs from Brown et al. (2009), the first 16 stars in Table 1. These stars fit well with the CWS and the Narm (Figure 3 and 4 in Lu et al. (2010)).

The following plot shows an Hammer-Aitoff projection of the sky with all 32 HVSs both the location of them now (open shapes) and the initial ejection direction (filled shapes). The thick line is a projection of the Narm and the thin line is a projection of the CWS.

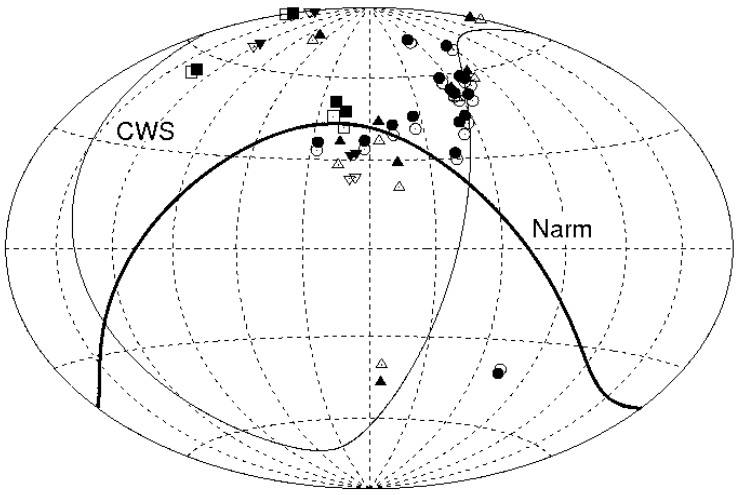

Figure 6: Hammer-Aitoff projection of all 32 HVSs in galactocentric coordinates, both the observed location of the stars (open shapes) and the initial ejection direction (filled shapes). Circles represent the 16 "confirmed" HVSs, squares represent the possible HVSs, the pyramids represent the possible bound HVSs and the upside-down pyramids represent the Svensson HVSs. All coordinates are found in Table 1

From Figure 6 and Table 1 we see that the initial ejection direction of all stars have a latitude that is higher (more negative if the latitude is negative) than the latitude of the stars today. As mentioned in Section 2.6 this is because the stars are pulled towards the Galactic plane by mainly the non-symmetric disk. Another thing that I notice is that the change in latitude is larger for star with latitudes that are initially small. This is reasonable since if the initial latitude is high the distance between the star and the disk becomes larger more quickly than if the initial latitude were lower. The third thing I notice is that the change in longitude is very small and that is also reasonable since even if the disk isn't spherically symmetric it is somewhat cylindrically symmetric and I use a cylindrically symmetric potential for the disk.

This seems fine but there is a problem: The CWS and the Narm contain massive stars, up to 20 $M_{\odot}$. Since massive stars evolve quickly the CWS and the Narm should be young structures, $\sim$ 6 Myr. But from Svensson et al. (2008) we know that the oldest HVSs are at least $\sim$ 170 Myr. The reason I say "at least" is because the star has travelled from the GC for that long time but it doesn't mean that the stars couldn't have lived for some time before ejection.

What I do is I improve their approach by using a larger sample of HVSs and I also use the initial ejection directions of the stars which aren't the same as the direction to the stars today as mentioned in Section 2.6. For me, the most important thing about the HVSs is the deflection angle. Since it's almost 180° the stars should stay in the same plane. By doing this I am able to, from the results of my simulations, see if their (Lu et al., 2010) conclusions are valid. Do the HVSs originate from these two disks as Lu et al. (2010) claim or are there other combinations of planes they could come from? I want to see if there are other combinations of two planes that fit equally well or even better.

Why two planes? We could easily use an arbitrary number of planes to fit all stars. But that is not interesting because it's not a result that gives me any new information. So from here on I assume that they come from two planes. Also since Lu et al. (2010) use two planes I use two planes so I can compare my results to their results and also test their conclusion that these two planes are a unique fit. If I find two other planes that have an equally good fit it will weaken the statement that all HVSs originate from one of these two planes.

I do best-fit simulations for four different sets of initial conditions:

First: I assume no deflection because of the Galactic potential, i.e. the trajectories of the HVSs are just straight lines.

- using the first 16 HVSs (as in Lu et al. (2010)).
- using all 32 HVSs.

Second: I use the code from Svensson et al. (2008) to get the trajectories and initial ejection direction of the HVSs.

- using the first 16 HVSs (as in Lu et al. (2010)).
- using all 32 HVSs.

To be able to separate the simulations from each other I name them depending on the set of initial conditions: Partial sample means that I used the first 16 stars in Table 1 and full sample means I used 32 stars. Undeflected means no deflection due to the Galactic potential and deflected means I allow for deflection because of the Galactic potential. So deflected partial sample means 16 stars with the deflection taken into account.

The results of my simulations can have different appearances. I divide them in three categories:

- There is only one good fit and thus the fit parameter distribution resembles a single mountain. I refer to this situation informally as Hawaii-type.
- There are several local minima and maxima in the fit parameter distribution so it resembles a mountain ridge. I refer to this situation informally as Himalaya-type.
- All combinations have ∼equally good/bad goodness-of-fit. In this situation the fit parameter distribution looks like a flat meadow, I refer to this situation informally as Skåne-type.

So what if the CWS and Narm combination is the only good one? How do we solve the problem with the age difference? For this question I have two different, possible solutions.

- Solution 1: There have been earlier existing disks with similar orientations. This leads to new questions: Where are they now? Why should they have the same orientation as the CWS and Narm?
- Solution 2: We accept that the HVSs all come from the CWS and Narm. Then we need continual rejuvenation of the disks over the past $\sim$200 Myr. But star formation is already constrained by tidal fields from the SMBH. Maybe sinking of cold gas which could form new stars? If so, would the orientation of the disks remain the same?

4 What I did

As mentioned in the section above for some of the simulations I need the initial ejection direction. To get the initial conditions for these simulations, i.e. where the trajectory is affected by the Galactic potential, I use the code from Svensson et al. (2008). To get the ejection direction of the stars, the code integrates the trajectories backwards in time in a model for the Galactic potential.

4.1 The Galactic potential

The Galactic potential model used is the Paczynski (1990) model which consists of two Miyamoto-Nagai potentials, one for the bulge and one for the disk, and one spherically symmetric potential for the halo.

Miyamoto-Nagai potentials are used for flattened systems and look like

$$\Phi(R,z) = -\frac{GM}{\sqrt{R^2 + \left(a + \sqrt{b^2+z^2}\right)^2}}$$

where a and b are constants that describes the shape of the system. For the bulge we have $a_b = 0.0$ pc, $b_b = 277$ pc and $M_b = 1.12 \times 10^{10}$ $\mathrm{M}_\odot$. For the disk we have $a_d = 3700$ pc, $b_d = 200$ pc and $M_d = 8.07 \times 10^{10}$ $\mathrm{M}_\odot$.

The halo potential looks like

$$\Phi_h(r) = -\frac{GM_c}{r_c}\left[\frac{1}{2}\ln\left(1+\frac{r^2}{r_c^2}\right) + \frac{r_c}{r}\arctan\left(\frac{r}{r_c}\right)\right]$$

where $r = \sqrt{R^2+z^2}$ is the distance between the object and the GC. The parameters used are: $M_c = 5.0 \times 10^{10}$ $\mathrm{M}_\odot$ and $r_c = 6000$ pc. Index c stands for core. Outside of the radius of the halo, $r_{halo} = 237$ kpc, the halo potential becomes

$$\Phi_h = -\frac{GM_{halo}}{r}$$

the halo mass used is $M_{halo} = 1.9 \times 10^{12}$ $\mathrm{M}_\odot$ (Wilkinson and Evans, 1999). So the potential used for the Galaxy is the sum of these three potentials. As seen in Table 1 the distance to the stars are smaller than the radius of the halo so we don't need to worry about the case when $r > r_{halo}$ right now. All values of the constants are taken from the Svensson et al. (2008) work.

4.2 The equations to be solved

To get the trajectory of a HVS we need to solve some equations of motion. The UVW-velocities are defined, in a cylindrical coordinate system (R, θ, z), as

$$\begin{cases} U = \frac{\mathrm{d}R}{\mathrm{d}t} \\ V = -R\frac{\mathrm{d}\theta}{\mathrm{d}t} \\ W = \frac{\mathrm{d}z}{\mathrm{d}t} \end{cases} \tag{15}$$

as we can see U is the radial velocity in the Galactic plane, V is the rotation speed in the same plane and W is the velocity perpendicular to the other two, i.e. the velocity in the z-direction. We also need the expressions for $\dot{U}$, $\dot{V}$ and $\dot{W}$, the acceleration in the different directions.

$$\begin{cases} \dot{U} = \frac{\mathrm{d}^2 R}{\mathrm{d}t^2} \\ \dot{V} = -\frac{\mathrm{d}R}{\mathrm{d}t}\frac{\mathrm{d}\theta}{\mathrm{d}t} - R\frac{\mathrm{d}^2\theta}{\mathrm{d}t^2} \\ \dot{W} = \frac{\mathrm{d}^2 z}{\mathrm{d}t^2} \end{cases} \tag{16}$$

In cylindrical coordinates a vector can be written as

$$\mathbf{x} = R\hat{\mathbf{e}}_R + z\hat{\mathbf{e}}_z$$

and if I differentiate this I get

$$\mathbf{v} = \frac{\mathrm{d}\mathbf{x}}{\mathrm{d}t} = \dot{R}\hat{\mathbf{e}}_R + R\dot{\hat{\mathbf{e}}}_R + \dot{z}\hat{\mathbf{e}}_z$$

In cartesian coordinates the radial unit vector is

$$\hat{\mathbf{e}}_R = \cos\theta\hat{\mathbf{e}}_x + \sin\theta\hat{\mathbf{e}}_y \Longrightarrow \mathrm{d}\hat{\mathbf{e}}_R = (-\sin\theta\hat{\mathbf{e}}_x + \cos\theta\hat{\mathbf{e}}_y)\,\mathrm{d}\theta \Longrightarrow \frac{\mathrm{d}\hat{\mathbf{e}}_R}{\mathrm{d}\theta} = \hat{\mathbf{e}}_\theta$$

similarly you can show that

$$\frac{\mathrm{d}\hat{\mathbf{e}}_\theta}{\mathrm{d}\theta} = -\hat{\mathbf{e}}_R$$

from these two equations I get

$$\begin{cases} \dot{\hat{\mathbf{e}}}_R = \frac{\mathrm{d}\hat{\mathbf{e}}_R}{\mathrm{d}\theta}\frac{\mathrm{d}\theta}{\mathrm{d}t} = \dot{\theta}\hat{\mathbf{e}}_\theta \\ \dot{\hat{\mathbf{e}}}_\theta = \frac{\mathrm{d}\hat{\mathbf{e}}_\theta}{\mathrm{d}\theta}\frac{\mathrm{d}\theta}{\mathrm{d}t} = -\dot{\theta}\hat{\mathbf{e}}_R \end{cases}$$

now I get the velocity as

$$\mathbf{v} = \dot{R}\hat{\mathbf{e}}_R + R\dot{\theta}\hat{\mathbf{e}}_\theta + \dot{z}\hat{\mathbf{e}}_z$$

the acceleration, $\mathbf{a}$, is the time derivative of this

$$\mathbf{a} = \frac{\mathrm{d}\mathbf{v}}{\mathrm{d}t} = \ddot{R}\hat{\mathbf{e}}_R + \dot{R}\dot{\hat{\mathbf{e}}}_R + \dot{R}\dot{\theta}\hat{\mathbf{e}}_\theta + R\ddot{\theta}\hat{\mathbf{e}}_\theta + R\dot{\theta}\dot{\hat{\mathbf{e}}}_R + \ddot{z}\hat{\mathbf{e}}_z =$$

$$= \left(\ddot{R} - R\dot{\theta}^2\right)\hat{\mathbf{e}}_R + \left(2\dot{R}\dot{\theta} + R\ddot{\theta}\right)\hat{\mathbf{e}}_\theta + \ddot{z}\hat{\mathbf{e}}_z$$

but I also know that the force is minus the gradient of the potential, $\mathbf{a} = -\nabla\Phi$, so from the above equation and eq. (16) I get

$$\begin{cases} \dot{U} = \frac{\mathrm{d}^2 R}{\mathrm{d}t^2} = \ddot{R} = -(\nabla\Phi)_R + R\dot{\theta}^2 = -(\nabla\Phi)_R + \frac{j_z^2}{R^3} = -\frac{\partial\Phi}{\partial R} + \frac{j_z^2}{R^3} \\ \dot{V} = -\frac{\mathrm{d}R}{\mathrm{d}t}\frac{\mathrm{d}\theta}{\mathrm{d}t} - R\frac{\mathrm{d}^2\theta}{\mathrm{d}t^2} = -\dot{R}\dot{\theta} - R\ddot{\theta} = (\nabla\Phi)_\theta + \dot{R}\dot{\theta} = \frac{1}{R}\frac{\partial\Phi}{\partial\theta} + \dot{R}\dot{\theta} \\ \dot{W} = \frac{\mathrm{d}^2 z}{\mathrm{d}t^2} = \ddot{z} = -(\nabla\Phi)_z = -\frac{\partial\Phi}{\partial z} \end{cases}$$

where $j_z = R^2\dot{\theta}$ is the angular momentum in the z-direction. Now I need the gradient of the potential. For the Miyamoto-Nagai potentials I get:

$$\frac{\partial}{\partial R}\Phi_{MN} = \frac{GMR}{\left(R^2 + \left(a + \sqrt{b^2 + z^2}\right)^2\right)^{3/2}}$$

$$\frac{\partial}{\partial \theta}\Phi_{MN} = 0$$

$$\frac{\partial}{\partial z}\Phi_{MN} = \frac{GM\left(a + \sqrt{b^2 + z^2}\right)z}{\sqrt{b^2 + z^2}\left(R^2 + \left(a + \sqrt{b^2 + z^2}\right)^2\right)^{3/2}}$$

And for the halo part we get:

$$\frac{\partial}{\partial R}\Phi_h = \frac{GM_c R}{r_c} \cdot \frac{r_c \arctan\left(\frac{r}{r_c}\right) - r}{r^3}$$

$$\frac{\partial}{\partial \theta}\Phi_h = 0$$

$$\frac{\partial}{\partial z}\Phi_h = \frac{GM_c z}{r_c} \cdot \frac{r_c \arctan\left(\frac{r}{r_c}\right) - r}{r^3}$$

We see that we have a rotational symmetry in θ. Inserting this in the equations for $\dot{U}$, $\dot{V}$ and $\dot{W}$ yields

$$\begin{cases} \dot{U} = -\frac{GM_b R}{\left(R^2+\left(a_b+\sqrt{b_b^2+z^2}\right)^2\right)^{3/2}} - \frac{GM_d R}{\left(R^2+\left(a_d+\sqrt{b_d^2+z^2}\right)^2\right)^{3/2}} - \\ \qquad -\frac{GM_c R}{r_c}\left[\frac{r_c \arctan\left(\frac{r}{r_c}\right)-r}{r^3}\right] + \frac{j_z^2}{R^3} \\ \dot{V} = -\frac{UV}{R} \\ \dot{W} = -\frac{GM_b\left(a_b+\sqrt{b_b^2+z^2}\right)z}{\sqrt{b_b^2+z^2}\left(R^2+\left(a_b+\sqrt{b_b^2+z^2}\right)^2\right)^{3/2}} - \\ \qquad -\frac{GM_d\left(a_d+\sqrt{b_d^2+z^2}\right)z}{\sqrt{b_b^2+z^2}\left(R^2+\left(a_d+\sqrt{b_d^2+z^2}\right)^2\right)^{3/2}} - \frac{GM_c z}{r_c}\left[\frac{r_c \arctan\left(\frac{r}{r_c}\right)-r}{r^3}\right] \end{cases} \tag{17}$$

The equation for $\dot{V}$ isn't really needed since it only gives the conservation of angular momentum. I derived these equations with some help from Binney and Tremaine (1987) and Kolb et al. (2000).

4.3 Get the initial ejection directions

With these equations I can get the trajectories of the stars if I know the initial locations and velocities. If I have these values I can integrate backwards numerically. For this I use the code from Svensson et al. (2008).

As argument the code takes a "guess" of the proper motions for the HVSs. The proper motion of a star is how much the star's position on the sky changes with time. It's measured in as yr^{-1} (arcseconds per year). The program makes a grid of proper motions centered around the guess for each star. Then it calculates the velocity of each star for all proper motions and integrates the trajectory of the stars backwards in time using the above mentioned potential. The equations ((15) and (17)) are solved with a Runge-Kutta 4th order method. This is done for all proper motions. Then I can get the trajectory with the smallest periapsis for each star and call them the best trajectories. So how do I get good guesses?

i) Start with the guess $\mu_\delta = \mu_\alpha = 0$ mas yr^{-1} and range 10 mas yr^{-1}. Then run `make_initial_grid.f` and `galtraj_s.f` to get the trajectories of the stars with these proper motions.

ii) Find the best trajectory, i.e. the one with smallest r_{min}, for each star with the program `PropFind.java`. This program also returns the initial proper motion of the trajectories.

iii) If r_{min} isn't good enough (since the potential doesn't separate the SMBH from the rest of the bulge I chose the limit to be 10 pc and not smaller) run the programs once again now with the proper motion grid centered at the new proper motion and with a smaller range.

iv) Repeat until r_{min} is small enough (< 10 pc).

4.4 Galactic coordinates to galactocentric coordinates

In most articles coordinates are given in Galactic coordinates (l, b). This coordinate system is centered in the Sun with longitude l and latitude b. $b = 0°$ is the Galactic plane and $l = 0°$ is the direction to the GC. Since I assume that all HVSs originate from the GC I need them in a galactocentric restframe, (l_{gc}, b_{gc}), so I need to transform them.

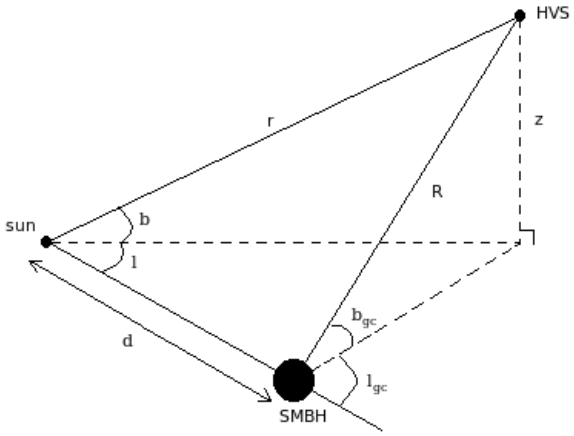

Figure 7: Coordinate transformation from Galactic coordinates to galactocentric coordinates. l and b are the Galactic coordinates and r is the heliocentric distance to the HVS. l_{gc} and b_{gc} are the coordinates in the galactocentric coordinate system and R is the distance between the GC and the HVS. z is the HVS's height above the Galactic plane and d is the distance between the Sun and the GC.

For all HVSs I have l, b, d and R (Brown et al. (2009), Brown et al. (2007)). I can get the height, z, in two different ways

$$r\sin b = z = R\sin b_{gc} \Longrightarrow r = R\frac{\sin b_{gc}}{\sin b} \tag{18}$$

Then the law of sines gives me

$$\frac{\sin l}{R\cos b_{gc}} = \frac{\sin\left(180^\circ - l_{gc}\right)}{r\cos b} = \frac{\sin l_{gc}}{r\cos b} \tag{19}$$

and the law of cosines yields

$$R^2\cos^2 b_{gc} = d^2 + r^2\cos^2 b - 2dr\cos b\cos l \tag{20}$$

If I insert eq. (18) in eq. (19) I get

$$\frac{\sin l}{R\cos b_{gc}} = \frac{\sin l_{gc}\sin b}{R\cos b\sin b_{gc}} \Longrightarrow \sin l_{gc} = \sin l\cdot\frac{\tan b_{gc}}{\tan b} \tag{21}$$

Then I insert eq. (18) in eq. (20) and get

$$R^2\cos^2 b_{gc} = d^2 + \frac{R^2\sin^2 b_{gc}}{\sin^2 b}\cos^2 b - 2d\frac{R\sin b_{gc}}{\sin b}\cos b\cos l \Longrightarrow$$

$$0 = \left(R^2 + \frac{R^2}{\tan^2 b}\right)\sin^2 b_{gc} - 2DR\frac{\cos l}{\tan b}\sin b_{gc} - R^2 + d^2$$

$$\Longrightarrow 0 = \sin^2 b_{gc} - \frac{d}{R}\sin(2b)\cos l\sin b_{gc} - \left(1 - \frac{d^2}{R^2}\right)\sin^2 b \tag{22}$$

Using equations (21) and (22) I obtain the coordinates in the galactocentric restframe, these are listed in Table 1. Now I have all initial conditions to get the initial ejection directions and when I get them I'm ready to find the best combination of planes for the HVSs.

4.5 Get the ejection direction in galactocentric coordinates

With the Svensson-code I have obtained good trajectories for each star and for each trajectory I have r, z, θ and the UVW-velocity at all points. With this I can get the ejection direction, (l_{gc}, b_{gc}), at r_{min}. In cylindrical polar coordinates, (R, θ, z), we have

$$\begin{cases} x = R\cos\theta \\ y = R\sin\theta \\ z = z \end{cases} \Longrightarrow \begin{cases} R = \sqrt{x^2+y^2} \\ \theta = \arctan\left(\frac{y}{x}\right) \\ z = z \end{cases} \tag{23}$$

Inserting eq. (23) in eq. (17) yields

$$\begin{cases} U = \frac{\mathrm{d}}{\mathrm{d}t}\left(\sqrt{x^2+y^2}\right) = \frac{1}{2}\frac{1}{\sqrt{x^2+y^2}}(2x\dot{x} + 2y\dot{y}) \\ V = -\sqrt{x^2+y^2}\frac{\mathrm{d}}{\mathrm{d}t}\left(\arctan\left(\frac{y}{x}\right)\right) = -\frac{\sqrt{x^2+y^2}}{1+\frac{y^2}{x^2}}\left(\frac{\dot{y}}{x} - \frac{y}{x^2}\dot{x}\right) = \\ \quad = -\frac{1}{\sqrt{x^2+y^2}}(x\dot{y} - y\dot{x}) \\ W = \frac{\mathrm{d}z}{\mathrm{d}t} = \dot{z} \end{cases} \tag{24}$$

From the second equation in (24) I get

$$\dot{y} = \frac{y}{x}\dot{x} - \frac{V\sqrt{x^2+y^2}}{x} \tag{25}$$

Insert this in the first equation in (24)

$$U = \frac{1}{\sqrt{x^2+y^2}}\left(x\dot{x} + \frac{y^2}{x}\dot{x} - \frac{Vy\sqrt{x^2+y^2}}{x}\right) \Longrightarrow \dot{x} = \frac{Vy+Ux}{\sqrt{x^2+y^2}}$$

Then I insert this in eq. (25) to get $\dot{y}$

$$\dot{y} = \frac{Vy^2}{x\sqrt{x^2+y^2}} + \frac{Uy}{\sqrt{x^2+y^2}} - \frac{V\sqrt{x^2+y^2}}{x} = \frac{Uy-Vx}{\sqrt{x^2+y^2}}$$

The normalized ejection direction is $\frac{\bar{\mathbf{v}}}{|\bar{\mathbf{v}}|}$ where $\bar{\mathbf{v}} = (\dot{x}, \dot{y}, \dot{z})$ which can be written as

$$\bar{\mathbf{v}} = \frac{1}{\sqrt{x^2+y^2}}\left(Vy+Ux, Uy-Vx, W\sqrt{x^2+y^2}\right) \tag{26}$$

and the square of the absolute value of this is

$$|\bar{\mathbf{v}}|^2 = \frac{1}{x^2+y^2}\left(V^2y^2 + 2UVxy + U^2x^2 + U^2y^2 - 2UVxy + V^2x^2 + \right.$$
$$\left. + W\left(x^2+y^2\right)\right) = U^2 + V^2 + W^2 \tag{27}$$

as expected since the velocity components are orthogonal to each other. Combining eq. (26) with eq. (27) we get the unit vector for the ejection direction

$$\hat{\mathbf{r}} = \frac{1}{\sqrt{x^2+y^2}\sqrt{U^2+V^2+W^2}}\left(Vy+Ux, Uy-Vx, W\sqrt{x^2+y^2}\right)$$

Now I finally can get the ejection direction in galactocentric coordinates

$$l_{gc} = \arctan\left(\frac{r_y}{r_x}\right) = \arctan\left(\frac{Uy-Vx}{Vy+Ux}\right) =$$
$$= \arctan\left(\frac{U\sin\theta - V\cos\theta}{V\sin\theta + U\cos\theta}\right)$$

$$b_{gc} = \arctan\left(\frac{r_z}{\sqrt{r_x^2+r_y^2}}\right) = \arctan\left(\frac{W\sqrt{x^2+y^2}}{\sqrt{(Vy+Ux)^2+(Uy-Vx)^2}}\right) =$$
$$= \arctan\left(\frac{W}{\sqrt{U^2+V^2}}\right)$$

4.6 My algorithms

Now I have all initial conditions for all four different simulations mentioned in Section 3. I want to find the best fitting combination of two planes. I use two different algorithms. They minimize the following quantities, the values of f_1 and f_2 are the goodness-of-fit for the combination of planes. The smaller value the better fit:

$$f_1 = \sum_i \min\left(|\hat{n}_1 \cdot \hat{e}_i|, |\hat{n}_2 \cdot \hat{e}_i|\right)$$

$$f_2 = \sum_i \min\left((\hat{n}_1 \cdot \hat{e}_i)^2, (\hat{n}_2 \cdot \hat{e}_i)^2\right)$$

$\hat{n}_1$ and $\hat{n}_2$ are the normals of the two planes, $\hat{e}_i$ is the unit vector of the ith HVS. The reason a small value on f_1 and f_2 is a better fit is because the normal to a plane is orthogonal to all vectors in that plane and if a star fits perfectly the unit vector of that star lies in the plane so the dot product becomes zero. So if all stars lie exactly in at least one of the planes the valus of f_1 and f_2 become zero. In the other extreme case, all HVSs have unit vectors that are parallel to the normals of the planes, the values of f_1 and f_2 become equal to the number of stars in the sample.

The program tries every combination of planes with integer values on the normal (l_{gc}, b_{gc}). I focus on the second algorithm since it is more similar to the one used in Lu et al. (2010). They use χ^2 statistics to find the best planes for the first 16 stars in Table 1.

5 What I found

As mentioned in Section 3 I do the simulations for four different sets of initial conditions: 16 (partial sample) or 32 (full sample) stars and with or without deflection of the trajectories due to the Galactic potential. Also I have two different quality-of-fit criteria but I focus on the second one since it's most like the one in Lu et al. (2010) and only present my results from those simulations.

5.1 Comparing with Lu et al. (2010)

Since we're interested in the Lu et al. (2010) results we start by comparing their results with the results we got from the case which has initial conditions that looks most like theirs: i.e. the undeflected partial sample of stars, 16 stars and no deflection.

Lu et al. (2010) find the following best-fit planes, i.e. the first 16 HVSs together with the CWS (thin line) and the Narm (thick line).

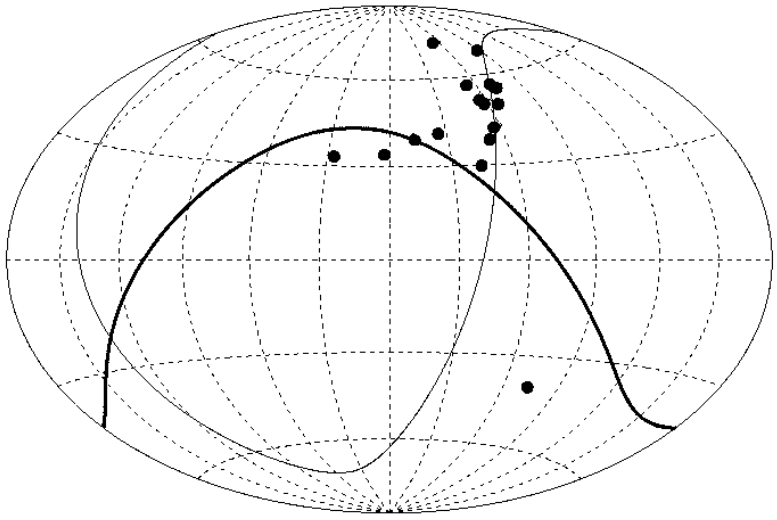

Figure 8: The 16 HVSs used in Lu et al. (2010) and the CWS and Narm plotted in an Aitoff-plot

The CWS has the normal $(l, b) = (310°, -18°)$ and the normal of the Narm is $(l, b) = (162°, -47°)$ The following is the best combination of planes that I get from my simulation.

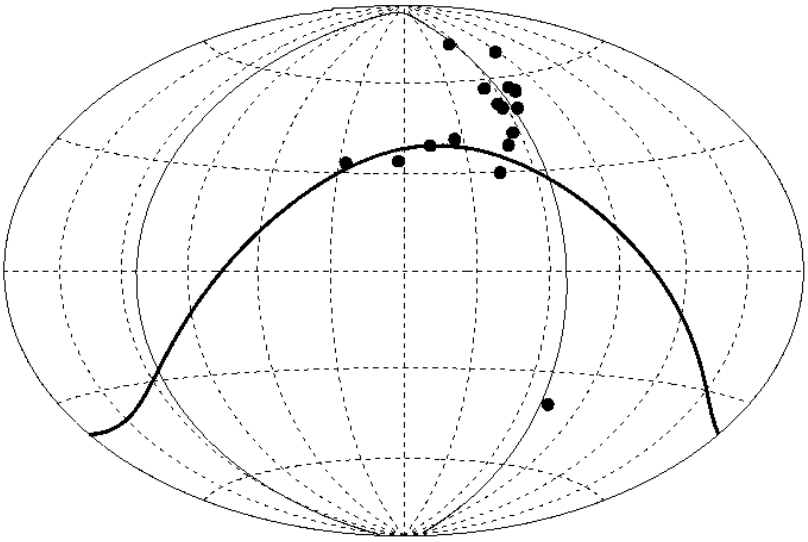

Figure 9: The 16 HVSs used in Lu et al. (2010) and the best combination of two planes from my simulations for the undeflected partial set of initial conditions plotted in an Aitoff-plot

The normals to these two planes are $(l, b) = (337°, 3°)$ for the thin line and $(l, b) = (195°, -51°)$ for the thick line. Comparing Figure 8 with Figure 9 we see that the planes are not the same but looking at the normals of the planes we see that they are not too different. It is also quite easy to see that the two planes from my simulations fit better than the CWS and the Narm, especially when you look at the star with negative latitude but even in general my two planes are better.

So the best combination of two planes for the first 16 stars without allowing for deflection by the Galactic potential are not the same as the two in Lu et al. (2010), but this doesn't tell me how much better the two new planes are. I have values on the goodness-of-fit for both combinations: $f_{CWS,Narm} \approx 0.362$ and $f_{new} \approx 0.100$ so the new planes are obviously better but it doesn't tell me much more than that. I still don't know how much better the new planes are, I don't know if it is a Hawaii-, Himalaya- or a Skåne-type of result. I need to get values on bad combinations too.

5.2 Description of a Dotplot

For each combination of planes I have five different values: The longitude and latitude of the first plane, the longitude and latitude of the second plane and finally a value of the goodness-of-fit, f. To be able to visualize differences between different combinations I make a coordinate system with the longitude of the normal to the first plane as the x-axis and the latitude of the normal to the first plane as the y-axis. Next I pick a point in this space, i.e. a normal to the first plane with fixed values, and I do a goodness-of-fit simulation with this plane as one of the planes. From this I get a second plane which is the plane that fits best together with the first one and a value on the goodness-of-fit for this combination. Next I make a dot on the coordinate system centered on the coordinates for the normal to the first plane. Then I repeat this for other points in the coordinate system untill I fill the plot with dots. To show the goodness-of-fit I assign a colour to the dot, the darker green the dot is the better fit I have. I have chosen to use normals to the first plane with values of l and b that are divisible by ten i.e. all combinations with $l_1 = 0°, 10°, 20°, \ldots, 350°, 360°$ and $b_1 = -90°, -80°, \ldots, 0°, \ldots, 80°, 90°$. An important thing to note is that the second plane

still has integer values of the longitude and latitude i.e. not only values that are divisible by ten.

I call this type of plot a Dotplot. An example of a Dotplot is shown in Figure 10. It shows the results after the simulations for the undeflected partial set of stars. Here I used the algorithm where I don't square the dot products between the normal to the plane and the unit vectors of the HVSs before I sum over all HVSs.

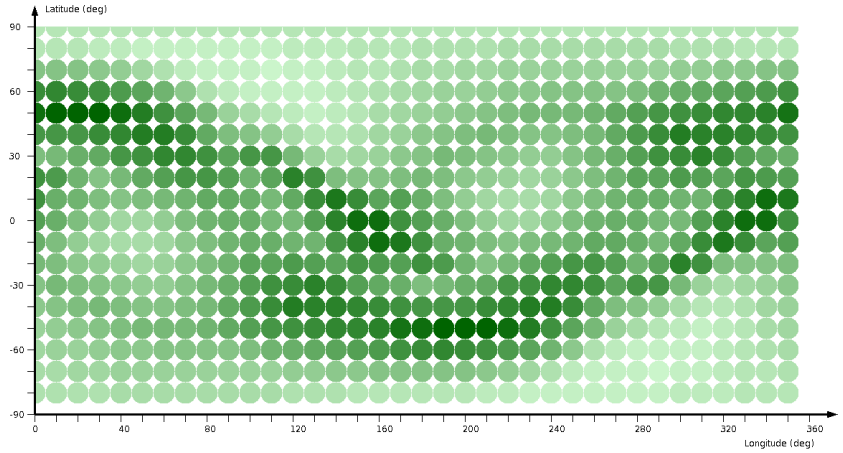

Figure 10: Dotplot for the undeflected partial set of initial conditions using the algorithm where I don't square the dot products between the normal to the plane and the unit vectors of the HVSs before I sum over all HVSs.

One thing you can see in Figure 10 is that we have a symmetry. Assume a plane has the normal (l, b) then that plane is the same as the plane with the normal $(l \pm 180°, -b)$, i.e. the vector which is anti-parallel to the first normal. I get this symmetry because physically it is the same plane but mathematically the normals to the two planes are anti-parallel to each other.

5.3 The results of my simulations

5.3.1 The case with the undeflected partial set of stars

So what are the results of my simulations? We saw in Figures 8 and 9 that the CWS and the Narm wasn't the best combination but how many combinations are better? To show my results I make some new plots for all four sets of initial conditions (see Section 3). As an example I discuss the plots made for the undeflected partial set of stars, i.e. the first 16 stars in Table 1 without taking the deflection due to the Galactic potential into account. The reason I use this and compare the other result mostly to the results of this case is because this is the simulation with initial conditions that are most like the initial conditions in Lu et al. (2010).

First of all I make a Dotplot, Figure 11,

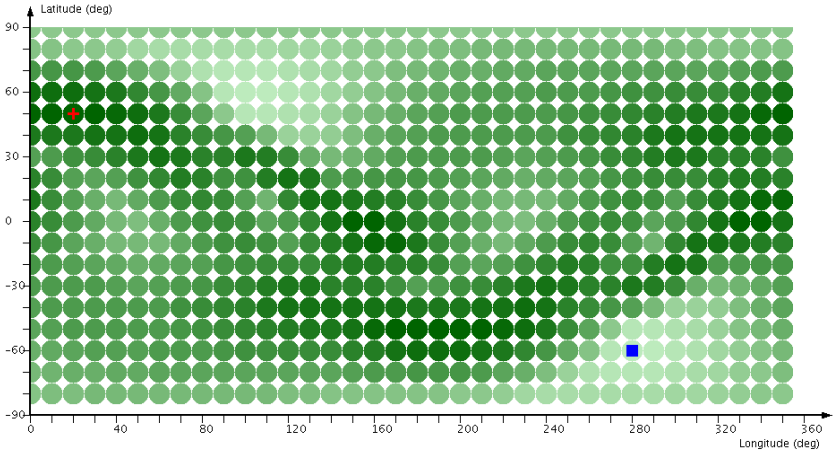

Figure 11: Dotplot for the undeflected partial sample initial conditions using the algorithm algorithm where I square the dot products between the normal to the plane and the unit vectors of the HVSs before I sum them. The red cross marks the combination of planes that have the best fit while the blue square marks the combination of planes with the worst fit in the Dotplot.

with this figure I can find the different combinations but since I want to know how good the results from Lu et al. (2010) are I make another Dotplot but this time I only mark the combinations that have a better fit than the CWS and Narm, Figure 12.

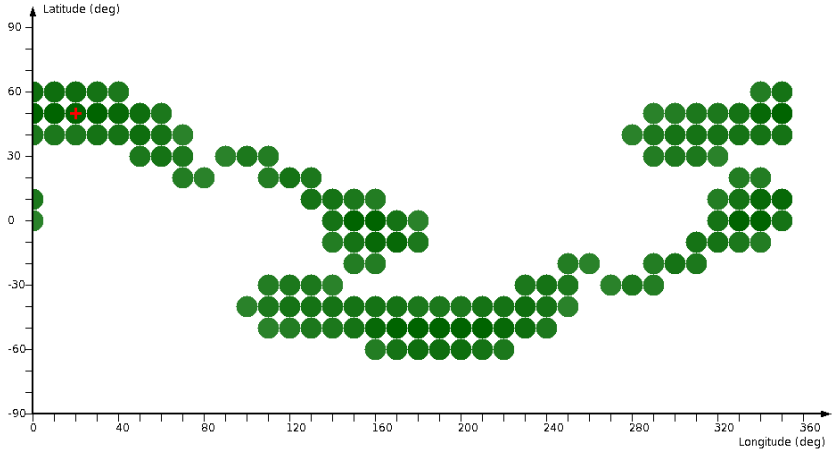

Figure 12: Dotplot with combinations that are better than the the result in Lu et al. (2010) plotted. The plot is for the undeflected partial sample initial conditions using the algorithm where I square the dot products between the normal to the plane and the unit vectors of the HVSs before I sum over all HVSs. The red cross marks the combination of planes that have the best fit in the Dotplot.

Next, I find the best and the worst combination from the Dotplots , Figure 11, and mark them. The best combination is marked with a red cross and the worst combination is marked with a blue square. I find the latitudes of the first planes in those two combinations. Then I plot the goodness-of-fit as a function of the longitude for the different combinations with those latitudes (solid and dashed lines in Figure 13). In the same plot I also mark all the combinations that are better than the CWS and Narm by plotting the goodness-of-fit of these combinations as a function of the longitude of the normal to the first plane, the crosses. Finally I also mark the goodness-of-fit for the CWS and Narm with a horizontal

dashed line. An important thing to note is that it is the low values on the goodness-of-fit that are good.

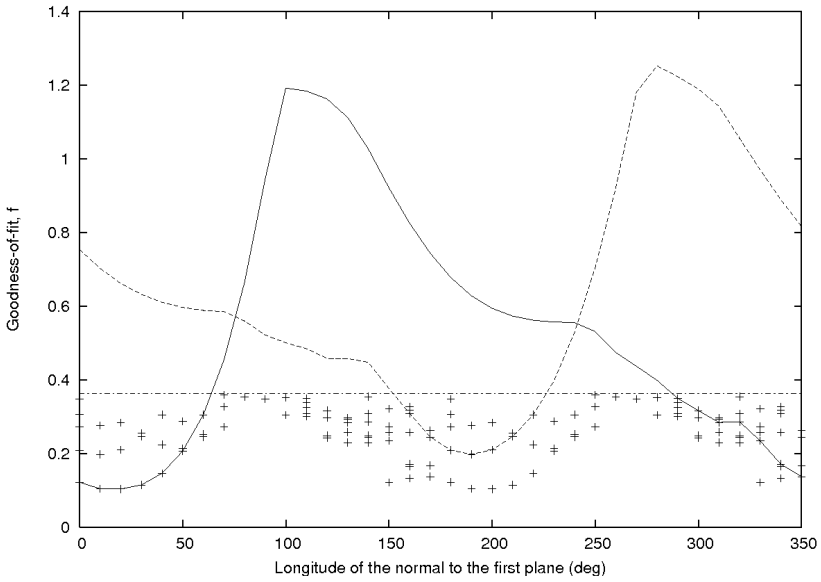

Figure 13: Plot showing the spread of goodness-of-fit values for combinations in the Dotplot for the undeflected partial sample initial conditions. The solid line is a plot of the combinations with a latitude of the first plane that is the same as the latitude of the first plane for the combination that has the best fit while the dashed line is the same except it is the latitude that contains the worst combination. The combinations of planes that have a better fit than the CWS and the Narm are also marked with crosses. The horizontal dashed line shows the goodness-of-fit for the CWS and Narm combination.

The final type of plot I have is a plot of the cumulative distribution of the goodness-of-fit over the planes, Figure 14. The cumulative distribution function is a function that, in my case, for a given combination of planes shows the probability that a randomly chosen combination of planes is better than the given one. In this plot I also mark what goodness-of-fit the CWS and Narm combination has so I can find how many other combinations of planes are better.

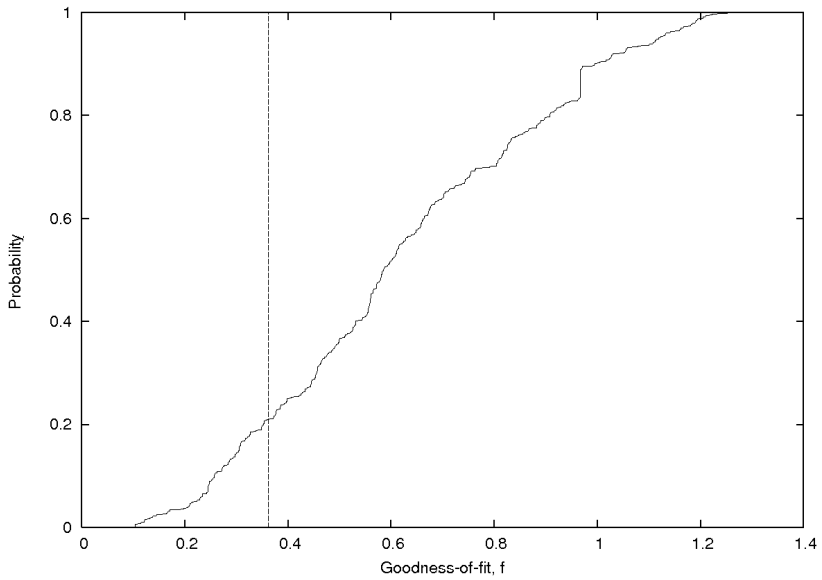

Figure 14: Cumulative distribution of the goodness-of-fit for different combinations of planes for the undeflected partial sample initial conditions.

In Figure 11 I see that there are differences between the different combinations but I still don't really know how big the differences are. From Figure 12 it is easy to see that there are quite a lot of combinations that are better than the existing structures (CWS and Narm). This can also be seen in Figure 13 since there are a number of crosses under the line representing the CWS and Narm combination. In the same plot I also note that there is some difference between the best combination and the "worst" combination so I would not say it has a Skåne-appearance. The reason I use "worst" and not worst is because the second plane in each dot is the one that gives the lowest goodness-of-fit together with the first plane so there are definitely combinations that are much worse. Figure 14 gives the fraction of combinations that have a better fit than the CWS and Narm. From the plot I get the value 0.21 so actually a quarter of the combinations are better. Again it is important to notice that the second plane is the best plane given the first one so it is not 21 % of all possible combinations that are better, just 21 % of the combinations in the Dotplot. With some imagination you could see that the curve in Figure 14 looks like a $\sqrt{x}$-function which is reasonable since the algorithm I use is a squared one. The conclusion for this simulation is that there definitely exist combinations of planes that are better than the CWS and Narm combination but it is still a good combination. So to answer the question from Section 3: The CWS and Narm combination is not the only combination of planes that fits well with the HVSs, at least not for this set of initial conditions.

5.3.2 The case with the deflected partial set of stars

In the result above I don't use the actual deflected ejection direction and also I have 16 more HVSs I can include. Next I show my results for the simulations with the deflected partial sample of stars, i.e. where I still only use the 16 stars used in Lu et al. (2010) but now I use the initial ejection direction of the HVSs and not their current location. I present the same four plots for these simulations:

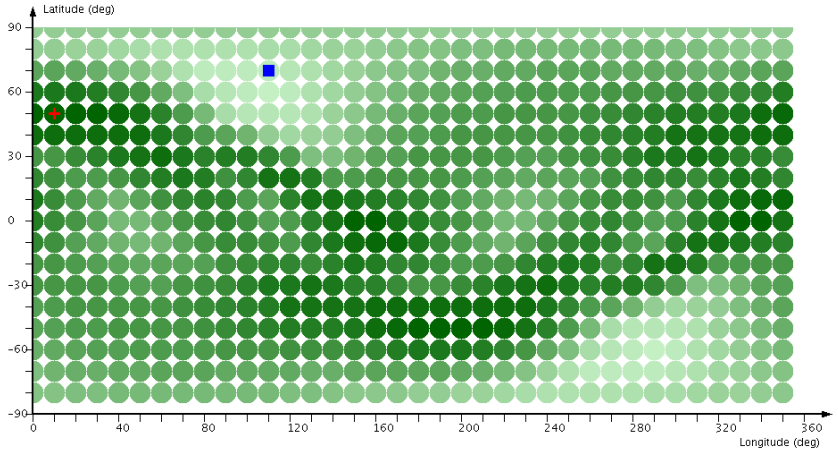

Figure 15: Dotplot for the deflected partial sample initial conditions using the algorithm where I square the dot products between the normal to the plane and the unit vectors of the HVSs before I sum over all HVSs. The red cross marks the combination of planes that have the best fit while the blue square marks the combination of planes with the worst fit in the Dotplot.

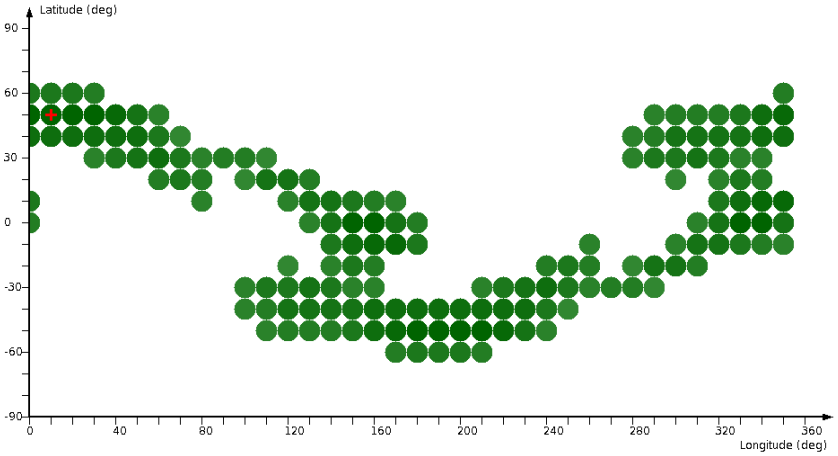

Figure 16: Dotplot with combinations that are better than the the result in Lu et al. 2010 Lu et al. (2010) plotted. The plot is for the deflected partial sample initial conditions using the algorithm where I square the dot products between the normal to the plane and the unit vectors of the HVSs before I sum over all HVSs. The red cross marks the combination of planes that have the best fit in the Dotplot.

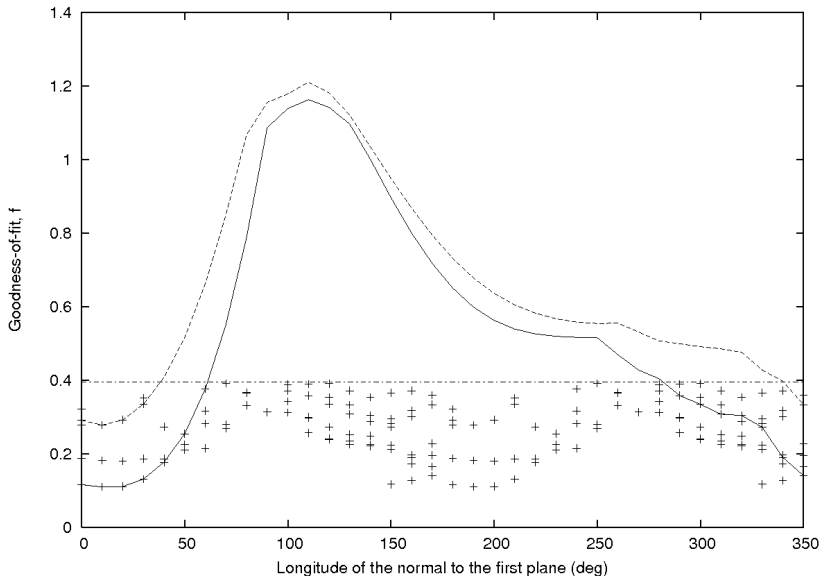

Figure 17: Plot showing the spread of goodness-of-fit values for combinations in the Dotplot for the deflected partial sample initial conditions. The solid line is a plot of the combinations with a latitude of the first plane that is the same as the latitude of the first plane for the combination that has the best fit while the dashed line is the same except it is the latitude that contains the worst combination. The combinations of planes that have a better fit than the CWS and the Narm are also marked with crosses. The horizontal dashed line shows the goodness-of-fit for the CWS and Narm combination.

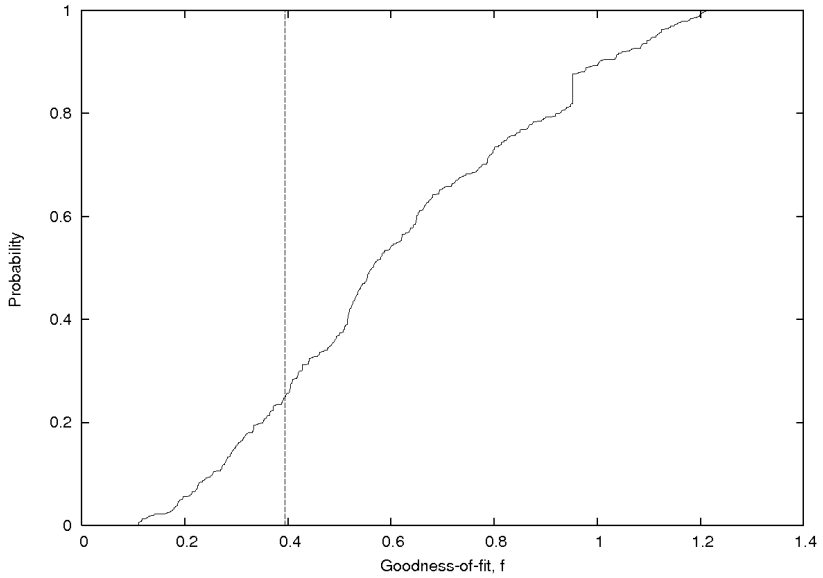

Figure 18: Cumulative distribution of the goodness-of-fit for different combinations of planes for the deflected partial sample initial conditions.

First I present the result from my simulations where I let the values of the longitudes and latitudes be integers, then I get the best combination to be $(196°, -48°)$ together with $(337°, 3°)$ to compare with the CWS and Narm $(310°, -18°)$ and $(162°, -47°)$. As you can

see these are not the same planes but they are similar to those found in the simulations for the undeflected partial sample of stars.

From the Dotplot above (Figure 15) you can see that it is very similar to the Dotplot for the undeflected partial simulation (Figure 11). In Figure 16 we see that there are a bit more combinations that are better. Also Figure 17 is similar to the corresponding plot for the undeflected partial case. The reason there is a difference between the curves is because I use two different latitudes for the curve with the "worst" combination. Even the cumulative distribution function is similar but now I get the fraction of combinations in the Dotplot that is better than the CWS and Narm to be 0.25. The conclusion of this is that if I add deflections I get some changes, the result from Lu et al. (2010) becomes a bit worse but it is not with much. I still wouldn't call it a Skåne-result but not a Hawaii-result either, there are more than one good combination.

5.3.3 The case with the undeflected full sample of stars

Ok, next I add 16 stars so I use all HVSs in my sample and return to use the assumption that the stars aren't affected by the Galactic potential. With these initial conditions I get the following results

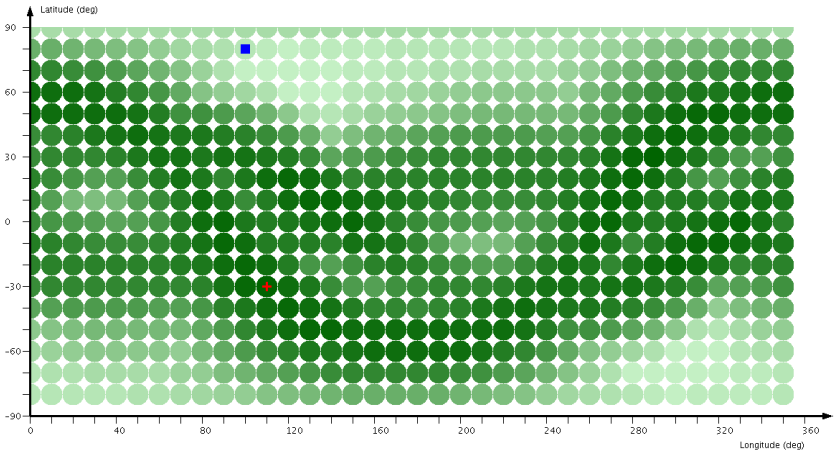

Figure 19: Dotplot for the undeflected full sample initial conditions using the algorithm where I square the dot products between the normal to the plane and the unit vectors of the HVSs before I sum over all HVSs. The red cross marks the combination of planes that have the best fit while the blue square marks the combination of planes with the worst fit in the Dotplot.

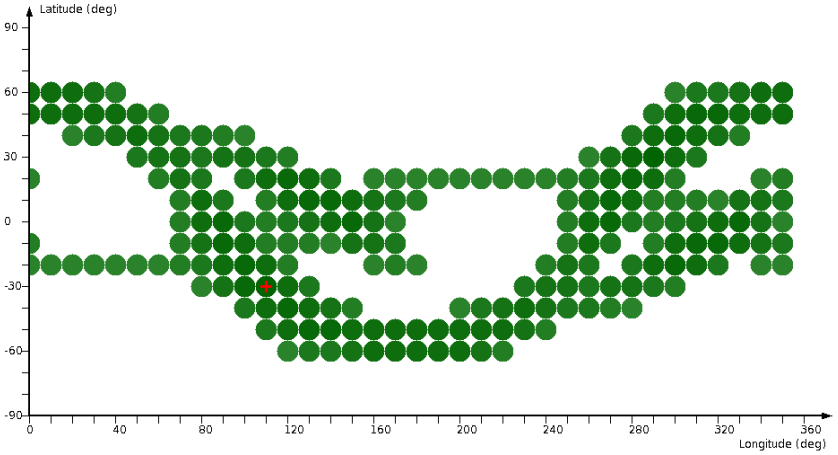

Figure 20: Dotplot with combinations that are better than the the result in Lu et al. 2010 Lu et al. (2010) plotted. The plot is for the undeflected full sample initial conditions using the algorithm where I square the dot products between the normal to the plane and the unit vectors of the HVSs before I sum over all HVSs. The red cross marks the combination of planes that have the best fit in the Dotplot.

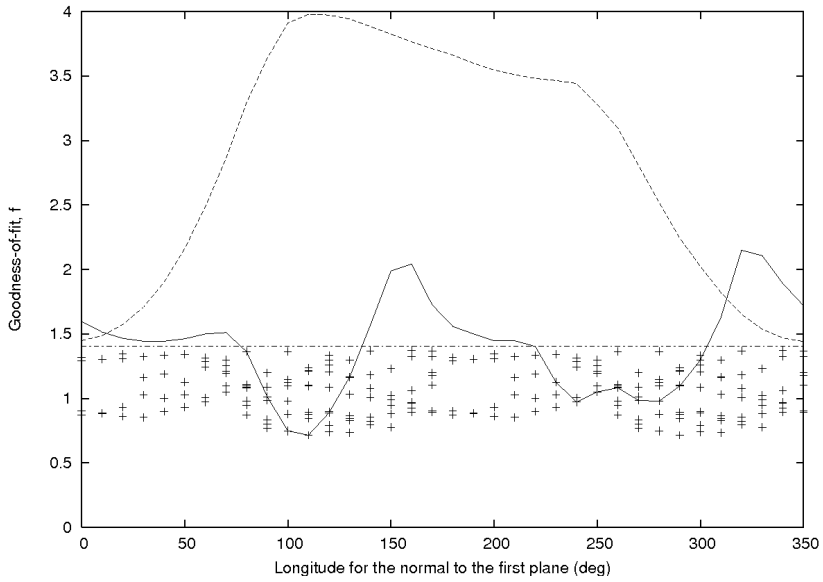

Figure 21: Plot showing the spread of goodness-of-fit values for combinations in the Dotplot for the undeflected full sample initial conditions. The solid line is a plot of the combinations with a latitude of the first plane that is the same as the latitude of the first plane for the combination that has the best fit while the dashed line is the same except it is the latitude that contains the worst combination. The combinations of planes that have a better fit than the CWS and the Narm are also marked with crosses. The horizontal dashed line shows the goodness-of-fit for the CWS and Narm combination.

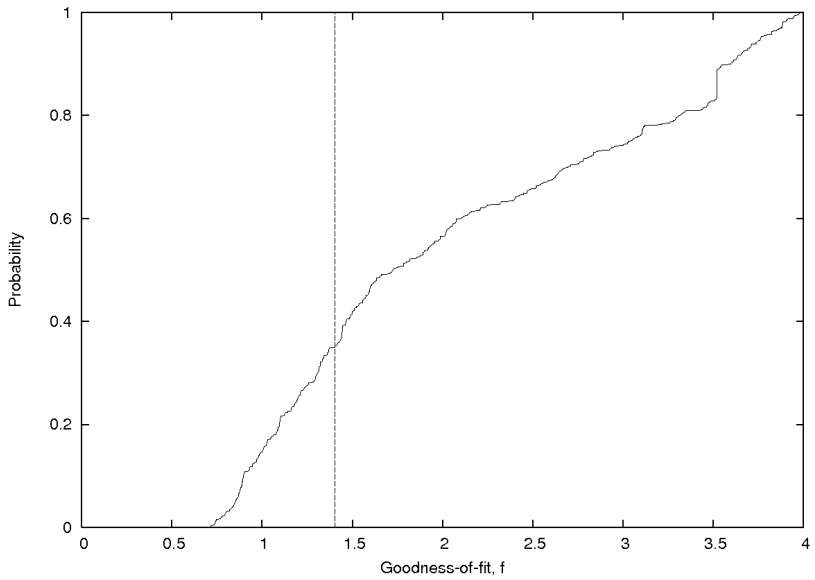

Figure 22: Cumulative distribution of the goodness-of-fit for different combinations of planes for the undeflected full sample initial conditions.

For these initial conditions I get the best combination of planes to be $(284°, 27°)$ together with $(305°, -15°)$ to compare with the CWS and Narm $(310°, -18°)$ and $(162°, -47°)$. As you can see the second plane is very similar to the CWS while the first plane dosn't look like the Narm.

The Dotplot (Figure 19) is again similar to the one for the undeflected partial set initial conditions (Figure 11) so it's not too outrageous to say that all 32 HVSs could be connected. One thing you see in Figure 21 is that the change in goodness-of-fit of good and bad combinations have increased from ~ 0.1 to ~ 0.7 for the best combination and from ~ 1.3 to ~ 4.0 for the worst combination by just doubling the number of stars. So I conclude that it makes a big difference if you add more stars to the sample. If we look at Figure 20 you see that it actually are fewer combinations that are better than the CWS and Narm than in the case of the deflected partial sample of stars. What you also could see in Figure 21 is that the curves have changed appearances. A reason for that is because I have different latitudes again. The cumulative distribution function has again the same shape and from it we read the fraction of combinations with goodness-of-fit lower than the CWS and Narm to be 0.35.

5.3.4 The case with the deflected full sample of stars

Finally we have the case where I use all 32 HVSs and allowing for the deflection, the deflected full set of stars. With these initial conditions I get the following results

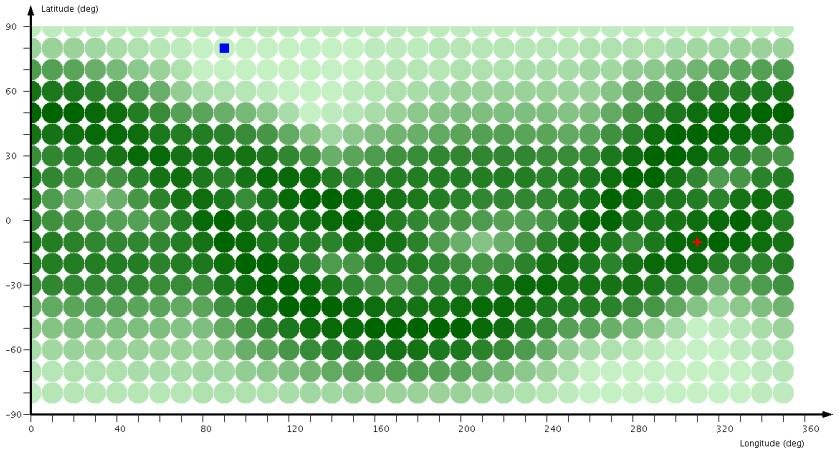

Figure 23: Dotplot for the deflected full sample initial conditions using the algorithm where I square the dot products between the normal to the plane and the unit vectors of the HVSs before I sum over all HVSs. The red cross marks the combination of planes that have the best fit while the blue square marks the combination of planes with the worst fit in the Dotplot.

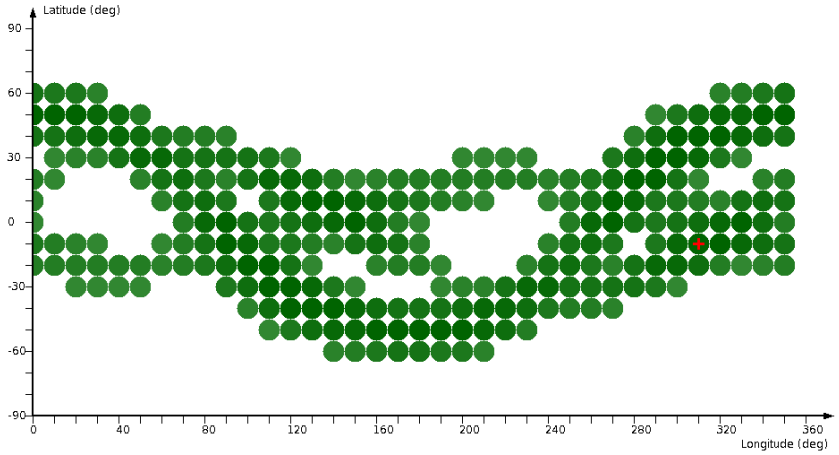

Figure 24: Dotplot with combinations that are better than the the result in Lu et al. 2010 Lu et al. (2010) plotted. The plot is for the deflected full sample initial conditions using the algorithm where I square the dot products between the normal to the plane and the unit vectors of the HVSs before I sum over all HVSs. The red cross marks the combination of planes that have the best fit in the Dotplot.

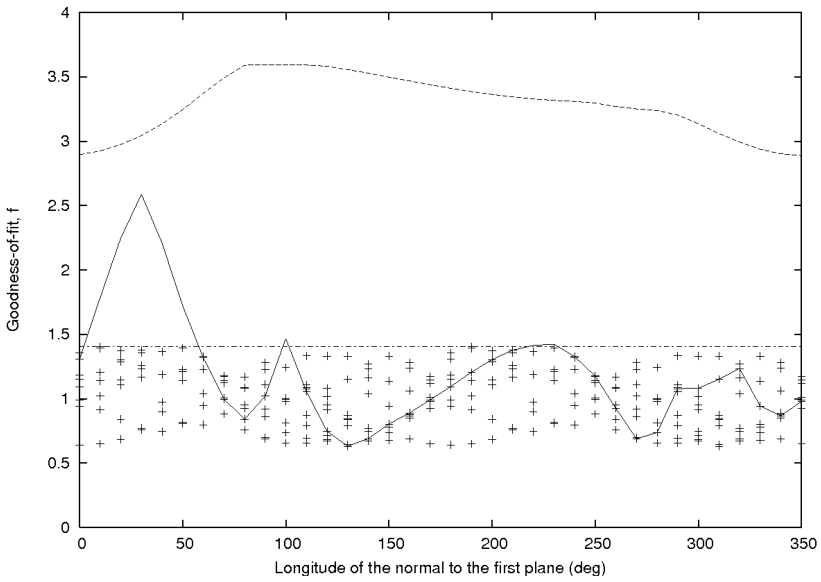

Figure 25: Plot showing the spread of goodness-of-fit values for combinations in the Dotplot for the deflected full sample initial conditions. The solid line is a plot of the combinations with a latitude of the first plane that is the same as the latitude of the first plane for the combination that has the best fit while the dashed line is the same except it is the latitude that contains the worst combination. The combinations of planes that have a better fit than the CWS and the Narm are also marked with crosses. The horizontal dashed line shows the goodness-of-fit for the CWS and Narm combination.

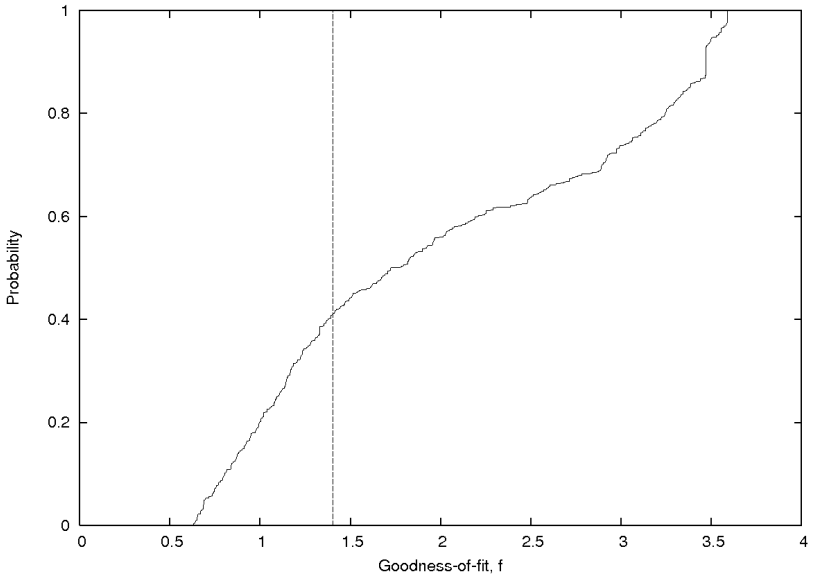

Figure 26: Cumulative distribution of the goodness-of-fit for different combinations of planes for the deflected full sample initial conditions.

These results are very similar to those of the undeflected full sample case with the exception there are more combinations that are better than the CWS and Narm, the fraction is now 0.41.

Next we look at the combination of planes that fits best with these stars: $(288°, 25°)$ together with $(306°, -13°)$ to compare with the CWS and Narm $(310°, -18°)$ and $(162°, -47°)$. Once again one of the planes is similar to the CWS while the other one is a bit more different to the Narm.

5.4 Conclusions

As a final conclusion I say that the existing disks, the CWS and the Narm, fit quite well with a lot of the HVSs. But it is not the best combination of planes in any of the simulations I have done. In particular, when you add more stars it becomes worse. Of the two planes, CWS and Narm, the CWS is the one that seems to cover most stars since planes similar to it appear as one of the best planes in both the undeflected full sample and deflected full sample simulations. So

- There are many combinations of planes with an equally good or better fit as seen from Figures 11-26.
- The phase-space is fairly flat with good fits for a wide range of planes. There are combinations better than the CWS and Narm combination for all possible values of the longitude of the normal to the first plane (see Figures 13, 17, 21 and 25)

Based on this I say that you can't claim that the HVSs definitely come from either the CWS or the Narm because they fit with the stars. There are too many other possible combinations that have a better or equally good fit. My answer on the question asked in Section 3 is: There are a lot of possible cobinations of two planes and the HVSs could come from either the CWS or the Narm but it's not something you can say for certain.

It would be good to have a larger sample of stars. Preferably they should be scattered over larger areas of the sky. Then it would be easier to see is there are any planar structures.

6 Further developments

In this section I discuss what would happen if we change some parameters of the problem and also how you could extend the project in the future.

6.1 Wider binaries

What would happen if we use binaries with larger separation between the stars? If you look at eq. (1)

$$v_{ej} = \sqrt{G\left(\frac{M_{BH}}{a_{BH}} - \frac{M_\star}{a_{bin}}\right)} \approx \sqrt{G\left(\frac{M_{BH}}{a_{BH}}\right)}$$

you see that this approximation would be even better for larger a_{bin} since then the initial binding energy in the binary would be even lower compared to the binding enegry of the captured star after ejection.

With a wider binary the binary separation Δr in eq. (8)

$$r_{bt} \approx \left(4\frac{M_{BH}}{m_b}\right)^{1/3} \Delta r$$

will be larger and the tidal disruption radius, r_{bt} for binaries will also be larger. If r_{bt} is larger the region where binaries are disrupted will be larger and more binaries will enter that region and be disrupted. That way more HVSs will be produced.

With a larger r_{bt} the semimajor axis of the captured star will also increase and the ejection velocity will be smaller. If the eccentricity, e, of the orbit of the captured star doesn't change I get $a_{BH} = \frac{r_{bt}}{1-e}$. So if I insert this in eq. (1) I get

$$v_{ej} \approx \sqrt{G\frac{M_{BH}}{a_{BH}}} = \sqrt{G\frac{M_{BH}\cdot(1-e)}{r_{bt}}} = \sqrt{G\frac{M_{BH}m_b^{1/3}\cdot(1-e)}{(4M_{BH})^{1/3}\,\Delta r}} = \sqrt{G\frac{M_{BH}^{2/3}m_b^{1/3}\cdot(1-e)}{4^{1/3}\Delta r}}$$

from this equation you can see that if I change the binary separation from $\Delta r \longrightarrow \alpha\Delta r$ the ejection velocity decreases with a factor $\frac{1}{\sqrt{\alpha}}$. If I start with a binary separation of $\Delta r = 0.1$ au, a mass of the SMBH $M_{BH} = 3.5\times10^6$ $M_\odot$, an eccentricity of the orbit of $e = 0.99$ and a binary mass $m_b = 6$ $M_\odot$ I get the ejection velocity to be $v_{ej} \approx 1500$ km s^{-1}. If I increase the separation by a factor of three so the separation is 0.3 au it becomes ~ 880 km s^{-1} and if I instead increase the separation by a factor of ten so the separation is 1 au it becomes ~ 500 km s^{-1}. One important thing to notice is that these limits on r_{bt} are how far out the binaries can be disrupted. They can come closer than that and then the captured star will become more tightly bound and the ejection speed will be higher so these are lower limits on the ejection speeds. But it's more likely that the binaries are disrupted at larger radii since the cross-section is bigger.

As I showed before a larger r_{bt} means that the closest approach, R_{min}, of the binary can be larger, I use $r_{bt} = R_{min}$, and from eq. (3)

$$\pi - \theta \approx \sqrt{\frac{2R_{min}}{GM_{BH}}}\left(v_\infty^{HVS} + v_\infty^{in}\right)$$

it seems like the approximation that the deflection angle is 180° will be less good. But as we saw before r_{bt} is proportional to Δr and $v_{ej} \propto \frac{1}{\sqrt{\Delta r}}$ which means that the deviation

from 180° for the deflection angle changes with a factor $\sqrt{\alpha}\frac{1}{\sqrt{\alpha}} = 1$ if $\Delta r \longrightarrow \alpha\Delta r$, i.e. the deviation from 180° is independent of binary separation. So if I use a binary separation of 0.1 au, the above calculated v_{ej} for that separation, neglect the velocity of the incomming binary and use a SMBH mass of 3.5×10^6 $M_\odot$ I get the deviation from 180° to be $\pi - \theta \approx 0.138 \approx 7.9°$. If I increase the binary separation the deflection angle stays the same since it's both dependant on the closest distance and the ejection velocity. This approximation becomes less good when the separation becomes larger, i.e. when the ejection velocity becomes smaller, since then the initial velocity makes a bigger difference.

Also from eq. (14)

$$v_{in} = \sqrt{\frac{2GM_{BH}}{d^2/r_{per} + d}}$$

we see that $v_{in,max}$ can be larger which also means that anti-parallel approximation will be less good.

6.2 More massive SMBH

If we have a more massive SMBH the tidal disruption radius of binaries, r_{bt}, will increase as we can see from eq. (8)

$$r_{bt} \approx \left(4\frac{M_{BH}}{m_b}\right)^{1/3} \Delta r$$

as we can see the disruption radius increases with a factor $\alpha^{1/3}$ if $M_{BH} \longrightarrow \alpha M_{BH}$. If I use a SMBH mass of 3.5×10^6 $M_\odot$, a binary mass of 6 $M_\odot$ and a binary separation of 0.1 au I get the break-up radius to be ~ 13 au. If I increase the mass of the SMBH to 35×10^6 $M_\odot$ the break-up radius becomes ~ 29 au and if the SMBH is really massive say 350×10^6 $M_\odot$ the break-up radius becomes ~ 62 au. So the binaries can be broken up further away from the SMBH. From Table II in Ferrarese and Ford (2005) you can see that the mass range 3.5×10^6 $M_\odot$-3.5×10^8 $M_\odot$ is reasonable.

The ejection velocity will also change since from eq. (1)

$$v_{ej} \approx \sqrt{G\frac{M_{BH}}{a_{BH}}}$$

that the ejection velocity is dependent on the mass of the SMBH but it is also dependent on how tightly bound the captured star is which also is dependant on the SMBH mass. If I assume the eccentricity of the captured star doesn't change when I change the mass of the SMBH I get $a_{BH} = \frac{r_{per}}{1-e}$ and taking the periapsis distance to be the tidal disruption radius I get

$$v_{ej} \approx \sqrt{G\frac{M_{BH}(1-e)}{r_{bt}}} \approx \sqrt{G\frac{M_{BH}m_b^{1/3}(1-e)}{(4M_{BH})^{1/3}\Delta r}} = \sqrt{G\frac{M_{BH}^{2/3}m_b^{1/3}(1-e)}{4^{1/3}\Delta r}}$$

So if I change the mass of the SMBH from $M_{BH} \longrightarrow \alpha M_{BH}$ the ejection speed changes with a factor $\alpha^{1/3}$. If I use a SMBH mass of 3.5×10^6 $M_\odot$, a binary mass of 6 $M_\odot$, a binary separation of 0.1 au and an eccentricity of the captured star's orbit of 0.99 I get the ejection velocity to be ~ 1500 km s^{-1}. If I take a ten times more massive SMBH the velocity changes to ~ 3300 km s^{-1} and if I take an even more massive SMBH say $M_{BH} = 350 \times 10^6$ $M_\odot$ the

ejection speed becomes ~ 7100 km s^{-1}. Since the SMBH in the Milky Way has quite low mass compared to other known SMBHs it is not impossible that there exist HVSs with these kind of speeds. When you have speeds of this magnitude you can't neglect them compared to the speed of light and have to start to take relativistic effects into account.

As I showed above $v_{ej} \propto M_{BH}^{1/3}$ which means that if the SMBH had been a dominating central body the distance the HVS could have travelled from the SMBH, r_{max}, would have scaled as $r_{max} \propto \frac{M_{BH}}{v_{ej}^2} \propto M_{BH}^{1/3}$. But the SMBH isn't massive compared to the rest of the Galaxy or even only the bulge. What I mean is that the thing that slows the HVSs down isn't the SMBH but the rest of the Galaxy. So the SMBH's effect on r_{max} is negligable compared to the contribution by the rest of the Galaxy and specially the part comming from the halo. This means that a larger SMBH mass increases the distance the HVSs travel since its mass is negligable compared to the mass of the rest of the Galaxy.

From eq. (3) I have

$$\pi - \theta \approx \sqrt{\frac{2R_{min}}{GM_{BH}}} \left(v_\infty^{HVS} + v_\infty^{in}\right)$$

if I take R_{min} to be the break-up radius, v_∞^{HVS} to be the ejection speed and neglect the velocity of the incoming binary, v_∞^{in}, I get

$$\pi - \theta \approx \sqrt{\frac{2\left(4M_{BH}\right)^{1/3}\Delta r}{Gm_b^{1/3}M_{BH}}} \cdot \sqrt{G\frac{M_{BH}^{2/3}m_b^{1/3}(1-e)}{4^{1/3}\Delta r}} = \sqrt{2(1-e)}$$

and if I, like I did before, use a eccentricity of $e = 0.99$ I get the deviation from 180° to be $\sim 8°$ like before. So the deflection angle is actually independant on the mass of the SMBH except you need a SMBH, a singularity that isn't disturbed by a binary, to create HVSs to begin with and also I make the assumption that the SMBH is the dominant body, $\frac{m_b}{r_{bt}} \ll \frac{M_{BH}}{a_{BH}}$.

The tidal disruption radius of single stars, r_t will increase as seen from eq. (13)

$$r_t \approx \left(2\frac{M_{BH}}{m_\star}\right)^{1/3} r_\star$$

Using the mass-radius relationship from Section 2.4 I get the radius of 3 $M_\odot$ star to be ~ 2.3 $R_\odot$. If I also use a SMBH mass of 3.5×10^6 $M_\odot$ and a stellar mass of 3 $M_\odot$ I get $r_t \sim 300$ $R_\odot \sim 1.4$ au. As seen from the above equation the tidal break-up radius of single stars increases with increasing SMBH mass. If $M_{BH} \longrightarrow \alpha M_{BH}$, $r_t \longrightarrow \alpha^{1/3} r_t$ so if I use a SMBH mass that is ten times higher I get the tidal break-up radius of a 3 $M_\odot$ to be ~ 650 $R_\odot \sim 3.0$ au and if I use a SMBH mass of 350×10^6 $M_\odot$ it becomes ~ 1400 $R_\odot \sim 6.5$ au

This and the fact that r_{bt} increases means that the area of disruption of binaries is moved a bit away from the SMBH but the space where this happens wil still be larger since the volume of a sphere is proportional to the radius cubed. If the mass increases with, say, a factor ten the volume goes from

$$V = \frac{4\pi}{3}r_{bt}^3 - \frac{4\pi}{3}r_t^3 \approx \frac{4\pi}{3}\left(4\frac{M_{BH}}{m_b}\left(\Delta r\right)^3 - 2\frac{M_{BH}}{m_\star}r_\star^3\right) \approx 10^4 \text{ (au)}^3$$

to $10V \approx 10^5$ (au)^2 since, as we can see in the above equation, the volume is proportional to the mass of the SMBH.

This also means that both $v_{in,min}$ and $v_{in,max}$ become larger (see eq. (14)

6.3 Other results of binary-SMBH interactions

HVSs are not the only possible result of binary-SMBH interactions. As I mentioned in Section 2.5 if the binary has a initial velocity that is too low it will come too close to the SMBH, $r_{per} < r_t$, and the stars will be disrupted. But even if we have a periapsis distance, closest approach, larger than r_t other things than HVS ejection can happen, e.g. collisions between the stars or even merging of the two stars if the stars come close enough to each other (Antonini et al., 2010). These things can happen even if $r_{per} > r_{bt}$. The eccentricity of the binary can grow with time making the minimum distance between the stars smaller with help of Kozai oscillations. Kozai oscillation is a relationship between the eccentricity in a binary and the binary's inclination to the orbital plane. If the binary is initially circular the maximum eccentricity possible is given by the following formula

$$e_{max} = \sqrt{1 - \frac{5}{3}\cos^2 j_{in}}$$

where j_{in} is the binary's initial incination to the orbital plane (Antonini et al., 2010).

A collision happens if the distance between the two stars in the binary is smaller than two star radii. Merging occurs if, during a collision, the relative velocity between the two stars is smaller than the escape velocity of the stars.

Antonini et al. (2010) found that HVSs are mainly produced in the first interaction between the binary and SMBH while collisions and mergers mostly occur after couple of interactions. This can be explained by the fact that the period of the Kozai oscillations are $\sim 2 - 120\times$ the orbit period of the binary around the SMBH, i.e. if it is in a bound orbit.

6.4 Errors

One big uncertainity I have is that I assume I have perfect data, i.e. I don't take any measurement errors into account. Also the heliocentric distances to the stars are calculated with an assumption that the HVSs have a certain mass. In a heliocentric coordinate system it's not too dangerous since errors in the distance are in the line of sight so the unit vectors of the stars don't change in this coordinate system. But when I change coordinate system (Section 4.4) I use the heliocentric distance to get l_{gc} and b_{gc} of a HVS, so if I change the value of the distance the value of the longitude and latitude will also change. Now I want to know how big the changes are compared to the deflections due to the Galactic potential. To investigate this I redo the coordinate transformations in Section 4.4 but this time I vary the distance to the stars by $\pm 10\%$, the range becomes $0.9R - 1.1R$ see Figure 7. I use 20 values in this range for each HVS and plot them as lines in an Aitoff-projection

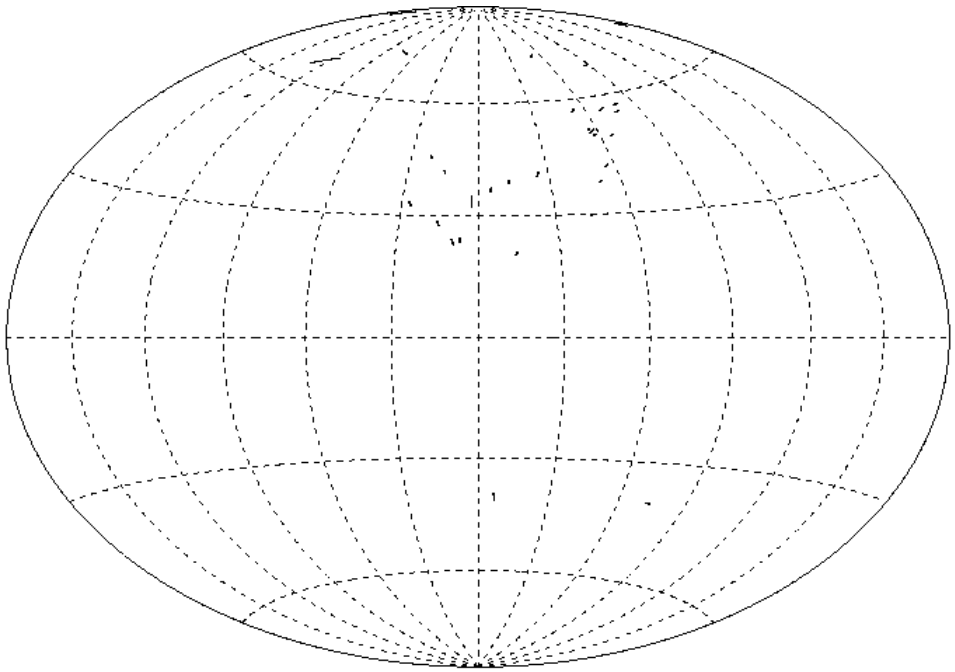

Figure 27: Hammer-Aitoff plot showing the range of galactocentric coordinates the HVSs have if the errors on the galactocentric distance are ±10%.

If we compare this figure with Figure 6 you see that the change in coordinates because of the uncertainity in distance are smaller than the changes when you take the Galactic potential into account. The differences are only a few degrees except for two stars where the difference is a bit larger, $|l_{gc,0.9R} - l_{gc,1.1R}|$ is for these cases $\sim 8°$ and $\sim 13°$. The reason these values are larger is because they are both quite close to the GC and are ejected with a longitude close to 90°.

6.5 Post-Newtonian extension

The HVSs move with extreme velocities, especially shortly after ejection. The ejection speed can be of the order 1 % of the speed of light. Because of this one extension of this project could be to add relativistic effects.

Antonini et al. (2010) study this using post-Newtonian simulations where they include terms up to order 2.5 in $\frac{v}{c}$. They do simulations of binary-SMBH interactions, both Newtonian and post-Newtonian and then compare them to see if there is any difference. The potential they use for the newtonian case is

$$V(r) = -\frac{GM_{BH}m_b}{r} + \frac{L^2}{2m_b r^2}$$

where r is the distance between the SMBH and the binary, m_b is the binary mass and L is the binary angular momentum. When they include post-Newtonian (PN) corrections they add

$$-\frac{GM_{BH}L^2}{c^2 m_b r^3}$$

to the potential, c is the speed of light. With this correction in eq. (14)) we see that for a given initial velocity the periapsis distance becomes smaller. So the PN corrections give higher limits on the initial velocities. The changes are of the order of a couple km s^{-1}.

When it comes to ejection of HVSs Antonini et al. (2010) found that PN corrections have some effect on the properties of the ejected stars. Especially for small binary separations and small apoapsis distances the mean value of the ejection velocity is a bit higher for the PN case. For larger separations and larger apoapsis distances the effect is smaller. This is not too surprising since from Section 6.1 we know that small binary separations lead to higher ejection velocities and then it's only natural that relativistic effects would be greater.

One other thing they find is that for the PN case the periapsis distances of the captured star are smaller than for the Newtonian case. This is expected since the velocities of the ejected stars are higher for the PN case the captured stars have to be more tightly bound to conserve energy.

The conclusion Antonini et al. (2010) draw is that the PN corrections is only important in the case where the binary separation is small. The effects they find are not large enough to be relevant to my project. I have other assumptions that give larger errors, e.g. the assumption that the deflection angle is 180° and the errors in the distances to the stars.

6.6 Dark matter halo

Another maybe more interesting thing to add to the project in the future is the possibility of a dark matter halo in the Milky Way that isn't spherically symmetric. An assymmetric halo is a destroyer of history, i.e. the more assymmetric it is the more deflected the trajectories of the HVSs will be. If the HVSs are deflected then the planar structure they have from the fact that the deflection angle is $\sim 180°$ and that they come from a disk will be destroyed. The reason the structure is destroyed is because the amount of deflection of the HVSs depends on the initial ejection directions as we saw in Figure 6 where only the bulge and disk were assymmetric. So why does an assymmetric halo make such a big difference? I already have two assymmetric parts to my potential: the bulge and the disk. The halo makes a big difference because the mass of the halo is much higher than the mass of the bulge and disk. Even though the density of stars in the halo is much smaller than the density of stars in the bulge or the disk the volume is so large that the mass of the halo becomes far greater than the mass of the bulge and the disk. The mass of the bulge and disk are $M_b = 1.12 \times 10^{10}$ $M_\odot$ and $M_d = 8.07 \times 10^{10}$ $M_\odot$ respectively while the mass of the halo is $M_{halo} = 1.9 \times 10^{12}$ $M_\odot$ (see Section 4.1) so it is the halo that causes the HVSs to slow down most. Were the halo assymmetric it would destroy the appearence that the HVSs come from two planes. This means that if we still have the planar structure of the HVSs when we look at the sky we could get some sort of upper limit of the assymmetry of the halo. This is if we assume that the HVSs originate from two planes/disks.

6.7 Metalicity of the HVSs

Yet another thing you could do, which is more observational, is to get the metalicities of the HVSs. If they come from the CWS they should have been produced at the same time so they should have roughly the same metalicity. If they have the same metalicity the solution is maybe the third solution mentioned in Section 3, i.e. the stars in the CWS and Narm have been reheated by tidal fields from the SMBH so that they look younger than they really are.

Acknowledgements

I want to thank my supervisors Melvyn B. Davies and Ross P. Church for first of all providing me with such an interesting project and secondly for all help they have given me. I also

want to thank them and Karl Svensson for the code for getting the initial ejection directions of the HVSs. Thanks also goes to Mohsen Farzone for enduring having the same office as me and getting interrupted in his work again and again to discuss my project.

References

Antonini, F., J. Faber, A. Gualandris, and D. Merritt (2010), "*Tidal Break-up of Binary Stars at the Galactic Center and its Consequenses.*" *ApJ*, **713**, 90–104.

Binney, J. and S. Tremaine (1987), *Galactic Dynamics*. Prinston University Press.

Brown, W. R., M. J. Geller, and S. J. Kenyon (2009), "*MMT Hypervelocity Star Survey.*" *ApJ*, **690**, 1639–1647.

Brown, W. R., M. J. Geller, S. J. Kenyon, and M. J. Kurtz (2005), "*Discovery of an Unbound Hypervelocity Star in the Milky Way Halo.*" *ApJ*, **622**, L33–L36.

Brown, W. R., M. J. Geller, S. J. Kenyon, M. J. Kurtz, and B. C. Bromley (2007), "*Hypervelocity Stars II. The Bound Population.*" *ApJ*, **660**, 311–318.

Davies, M. B. and A. King (2005), "*The Stars of the Galactic Center.*" *ApJ*, **624**, L25–L27.

Edelmann, H., R. Napiwotzki, U. Heber, N. Christlieb, and D. Reimers (2005), "*HE 0437-5439: An Unbound Hypervelocity Main-sequence B-type Star.*" *ApJ*, **634**, L181–L184.

Eisenhauer, F., R. Genzel, T. Alexander, R. Aubter, T. Paumard, T. Ott, A. Gilbert, S. Gillessen, M. Horrobin, S. Trippe, H. Bonnet, C. Dumas, N. Hubin, A. Kaufer, M. Kissler-Patig, G. Monnet, S. Ströbele, T. Szeifert, A. Eckart, R. Schödel, and S. Zucker (2005), "*Sinfoni in the Galactic Center: Young Stars and Infrared Flares in the Central Light-Month.*" *ApJ*, **628**, 246–259.

Ferrarese, L. and H. Ford (2005), "*Supermassive Black Holes in Galactic Nuclei: Past, Present and Future Research.*" *SSR*, **116**, 523–624.

Hills, J. G. (1988), "*Hyper-velocity and tidal stars from binaries disrupted by a masive Galactic black hole.*" *Nature*, **331**, 687–689.

Kolb, U., M. B. Davies, A. King, and H. Ritter (2000), "*The violent past of Cygnus X-2.*" *MNRAS*, **317**, 438–446.

Lu, Y., F. Zhang, and Q. Yu (2010), "*On the Spatial Distribution and the Origin of Hypervelocity Stars.*" *ApJ*, **709**, 1356–1361.

Paczynski, B. (1990), "*A Test of the Galactic Origin of Gamma-Ray Bursts.*" *ApJ*, **348**, 485–494.

Paumard, T., R. Genzel, F. Martins, S. Nayakshin, A. M. Beloborodov, Y. Levin, S. Trippe, F. Eisenhauer, T. Ott, S. Gillessen, R. Aubter, J. Cuadra, T. Alexander, and A. Sternberg (2006), "*The Two Young Star Disks an the Central Parsec of the Galaxy: Properties, Dynamics and Formation.*" *ApJ*, **1011**, 1011–1035.

Svensson, K. M., R. P. Church, and M. B. Davies (2008), "*The nature of hypervelocity as inferred from their Galactic trajectories.*" *MNRAS*, **383**, L15–L19.

Wilkinson, M. I. and N. W. Evans (1999), "*The Present and Future Mass of the Milky Way Halo.*" *MNRAS*, **310**, 645–662.

Zhao, J.-H., M. R. Morris, W. M. Goss, and T. An (2009), "*Dynamics of Ionized Gas at the Galactic Center: Very Large Array Observations of the Three-dimensional Velocity Field and Location of the Ionized Streams in Sagittarius A West.*" *ApJ*, **699**, 186–214.